

Tidal disruption rate of stars by supermassive black holes obtained by direct N-body simulations

M. Brockamp^{1*†}, H. Baumgardt^{2‡}, P. Kroupa¹

¹ *Argelander Institute for Astronomy (AIfA), Auf dem Hügel 71, D-53121 Bonn, Germany*

² *School of Mathematics and Physics, University of Queensland, Brisbane, QLD 4072, Australia*

Received / Accepted

ABSTRACT

The disruption rate of stars by supermassive black holes (SMBHs) is calculated numerically with a modified version of Aarseth’s NBODY6 code. Equal-mass systems without primordial binaries are treated. The initial stellar distribution around the SMBH follows a Sérsic $n = 4$ profile representing bulges of late type galaxies as well of early type galaxies without central light deficits, i.e. without cores. In order to infer relaxation driven effects and to increase the statistical significance, a very large set of N-body integrations with different particle numbers N , ranging from 10^3 to $0.5 \cdot 10^6$ particles, is performed. Three different black hole capture radii are taken into account, enabling us to scale these results to a broad range of astrophysical systems with relaxation times shorter than one Hubble time, i.e. for SMBHs up to $M_\bullet \approx 10^7 M_\odot$. The computed number of disrupted stars are driven by diffusion in angular momentum space into the loss cone of the black hole and the rate scales with the total number of particles as $\frac{dN}{dt} \propto N^b$, where b is as large as 0.83. This is significantly steeper than the expected scaling $\frac{dN}{dt} \propto \ln(N)$ derived from simplest energy relaxation arguments. Only a relatively modest dependence of the tidal disruption rate on the mass of the SMBH is found and we discuss our results in the context of the $M_\bullet - \sigma$ relation. The number of disrupted stars contribute a significant part to the mass growth of black holes in the lower mass range as long as a significant part of the stellar mass becomes swallowed by the SMBH. This also bears direct consequences for the search and existence of IMBHs in globular clusters. For SMBHs similar to the galactic center black hole Sgr A*, a tidal disruption rate of 55 ± 27 events per Myr is deduced. Finally relaxation driven stellar feeding can not account for the masses of massive black holes $M_\bullet \geq 10^7 M_\odot$ in complete agreement with conventional gas accretion and feedback models.

Key words: black hole physics, spherical galaxies, Sérsic profiles, methods: N-body simulations, gravitational dynamics

1 INTRODUCTION

The evolution of supermassive black holes (SMBHs) and their host galaxies is at present one of the key problems of astrophysics. Motivated by empirically found scaling relations between properties of galaxies in terms of velocity dispersion σ (Gebhardt et al. 2000; Ferrarese & Merritt 2000; Gültekin et al. 2009), luminosity

L (Kormendy & Richstone 1995; Ferrarese & Ford 2005), bulge mass M_{Bulge} (Magorrian et al. 1998; Häring & Rix 2004), central light deficit L_{def} (Lauer et al. 2007; Kormendy & Bender 2009; Hopkins & Hernquist 2010), total number of globular clusters N_{GC} (Burkert & Tremaine 2010) and the mass of their central black holes M_\bullet , there is a substantial need to understand the related evolution of both SMBHs and their hosts. In order to constrain galaxy formation models and to answer the question as to what powers the growth of SMBHs over cosmic times, all forms of matter which are accreted must be taken into account. This becomes more urgent as recent studies have found evidence for deviations from the general scaling relations for the most-massive and for the least-massive black holes

* brockamp@astro.uni-bonn.de

† Member of the International Max Planck Research School (IMPRS) for Astronomy and Astrophysics at the Universities of Bonn and Cologne

‡ h.baumgardt@uq.edu.au

(Lauer et al. 2007; Gebhardt et al. 2011; Kormendy et al. 2011).

Gas accretion is thought to be the most dominant driver of SMBH growth (Soltan 1982). Modern studies (Yu & Tremaine 2002) estimate the black hole mass density from the spatial distribution and from the measured stellar velocity dispersions in elliptical galaxies in combination with the $M_\bullet - \sigma$ relation. The SMBH mass density is then compared with the observed quasar luminosity function in order to yield constraints on the accretion efficiency parameter ϵ as well as on the growth history. In order to make these studies even more accurate, the impact of other feeding modes like merging supermassive black holes and stellar captures must also be taken into account. Simultaneously the luminous gas accretion history of low-mass SMBHs ($M_\bullet \approx 10^5 - 10^7 M_\odot$) is harder to measure especially at large redshifts as they never approach luminosities comparable to those of quasars. It is even plausible that low-mass SMBHs gain most of their mass by tidal disruption events (Milosavljević et al. 2006). Therefore it is important to infer the stellar capture rate for as many astrophysical systems of interest as possible, for all relevant SMBH masses using both theoretical and when possible numerical approaches. In order to avoid confusion regarding the terminology of the capture and disruption rate we note that the former expression is used for the general number of stars/particles which are either swallowed as a whole or disrupted outside the event horizon in a given time, i.e. independent of the mass of the SMBH. The latter one is explicitly used for situations in which stars are tidally disrupted before they would enter the event horizon.

In this paper we present the disruption rate of stars by SMBHs with masses in the lower range up to $M_\bullet \lesssim 10^7 M_\odot$ embedded inside realistic stellar density profiles. These results are obtained by self-consistent direct N-body integrations and increase the hitherto probed region of direct numerically inferred disruption rates. Pioneered by Baumgardt et al. (2004a,b, 2006) for intermediate-mass black holes (IMBHs) at the centers of globular clusters, our calculations can be applied to a larger sample of systems. Our findings should be regarded as complementary to other contributions (Duncan & Shapiro 1983; Magorrian & Tremaine 1999; Amaro-Seoane et al. 2004) where the impact of tidal disruption events is shown to be significant and therefore should not be neglected in considering the question of what powers the growth of black holes.

There are several mechanism by which stars are driven into the loss cone of a black hole. In spherical stellar distributions, where the relaxation time T_{rel} is comparable to or smaller than the present age of the universe¹ t_0 (Freitag et al. 2008), two-body relaxation induces a steady change in the angular momentum space distribution of stars such that some of them will drift

¹ For the purposes of this study we do not discriminate between t_0 and one Hubble time H_0^{-1} and assume $H_0^{-1} \approx t_0 = 13.7 \cdot 10^9$ yr (Komatsu et al. 2009).

to very eccentric orbits with pericentre distances smaller than the black hole capture radius (Frank & Rees 1976; Lightman & Shapiro 1977). In much larger systems like the most-massive elliptical galaxies which are thought to be triaxial in shape (Kormendy & Bender 1996), stars on box orbits can cross the central region arbitrary close to the SMBH (Binney & Tremaine 2008) such that they become disrupted or swallowed as a whole for the case of a very massive SMBH. Merritt & Vasiliev (2010) concluded that the feeding mode of very massive SMBHs, like M87 (Gebhardt & Thomas 2009), is currently dominated by stellar captures. The true rates could be even higher since their analysis takes only stellar orbits within the black hole influence radius r_h into account, whereas stars within the loss cone but from much further away should reach the black hole, too, as long as the critical radius r_{crit} (a quantity which is defined in Eq. 3) remains larger than r_h . Norman & Silk (1983); Poon & Merritt (2001, 2002); Merritt & Poon (2004); Berczik et al. (2006) provide additional information on the dynamics of SMBHs and stellar capture rates in triaxial potentials.

Observed disruption events (Ulmer 1999; Komossa 2002; Halpern et al. 2004; Komossa et al. 2004; Esquej et al. 2008; Gezari et al. 2008; Cappelluti et al. 2009; Gezari et al. 2009; Komossa et al. 2009; van Velzen et al. 2010 and references therein), support the view that tidal disruptions contribute to the growth history of SMBHs. To which magnitude this is the case is a major aspect of this study.

The paper is organized as follows. In § 2 we will shortly explain the concept by which stars are driven by angular momentum diffusion into the “loss cone” of the SMBH. This formalism is applied to spherical stellar distributions with arbitrary slope parameters of the density profile. § 3 describes the NBODY6 code that we used. We will specify the scale-free models and motivate the very large set of performed simulations required to infer the disruption rate of stars by SMBHs in the nuclei of galaxies. The results will be given in § 4 while more detailed information regarding the dynamics of the simulations will be part of § 5. In § 6 the procedure how to scale the obtained results to realistic astrophysical systems as well as the number of expected tidal disruption events will be specified. A critical discussion of potential error sources in § 7 is followed by a summary of our main findings in § 8.

2 THEORY

Frank & Rees (1976) calculate that massive black holes can grow not only by swallowing stars which lose their energy via dynamical relaxation, but also by swallowing stars on very eccentric orbits i.e. stars with low angular momentum. The change of the stellar distribution in angular momentum space is expected to progress much faster than the change in energy space for stars within the critical radius r_{crit} . Considering stars with very low angular momentum and pericentre distances smaller than the capture radius of the black hole, the velocity vectors of these stars must be aligned very narrowly. This narrow region is known as the loss cone. It only reflects the geometry in velocity space and is characterized

by the loss cone angle θ_{lc} whose symmetry axis is directed towards the position of the black hole. For distances below the influence radius r_H of the black hole where the velocity profile follows a Keplerian one ($\propto r^{-0.5}$), θ_{lc} is given by

$$\theta_{lc} \propto \left(\frac{2r_{cap}}{3r} \right)^{\frac{1}{2}} \quad (1)$$

according to Frank & Rees (1976). For $r \geq r_H$ a slightly different expression has to be used. At the moment we leave it undefined if the stars are disrupted before entering the horizon of the black hole or if they are swallowed as a whole. A general capture radius r_{cap} can be specified for all purposes (Novikov & Frolov 1989; Binney & Tremaine 2008; see also Appendix A). In perfectly spherical potentials i.e. potentials where no torques from anisotropic matter distributions can induce an additional supply of stars, all stars on loss cone orbits would be consumed within one orbital time scale t_{cross} . However, dynamical relaxation between stars causes a steady change of the stellar distribution in angular momentum space and therefore changes in the velocity vectors by small amounts θ_{Diff} per crossing time (Frank & Rees 1976):

$$\theta_{Diff} \propto \left(\frac{t_{cross}}{t_{rel}} \right)^{\frac{1}{2}}. \quad (2)$$

The critical radius r_{crit} which is the characteristic distance to the black hole where the drift in the velocity vector of a star due to dynamical relaxation within one crossing time is of the same order as θ_{lc} is therefore defined as:

$$\left. \frac{\theta_{lc}}{\theta_{Diff}} \right|_{r=r_{crit}} = 1 \quad (3)$$

Assuming a number density profile² $n(r) = n_0 r^\alpha$ within $r_{crit} \leq r_H$ and considering only equal mass stars, an expression for the critical radius

$$r_{crit} \propto \left(\frac{r_{cap} M_\bullet^2}{M_\star^2 n_0} \right)^{\frac{1}{4+\alpha}} \quad (4)$$

is obtained by inserting Eq. 1 and Eq. 2 into Eq. 3. Spitzer's relaxation formula (Spitzer & Harm 1958; Spitzer 1987) is used for the relaxation time t_{rel} . The Coulomb logarithm is neglected.

The stellar capture rate can be derived by using eq. 17 from Frank & Rees (1976)³:

$$\dot{C} \propto \left. \frac{\theta_{lc}^2 r^3 n(r)}{t_{cross}} \right|_{r=r_{crit}} = \left. \frac{\theta_{Diff}^2 r^3 n(r)}{t_{cross}} \right|_{r=r_{crit}}, \quad (5)$$

For a density profile $n(r \leq r_{crit}) = n_0 r^\alpha$ the stellar disruption rate \dot{C} is obtained by substituting $r = r_{crit}$:

$$\dot{C} \propto G^{\frac{1}{2}} M_\bullet^{\frac{1}{2}} r_{cap} n_0 \left(\frac{r_{cap} M_\bullet^2}{M_\star^2 n_0} \right)^{\frac{0.5+\alpha}{4+\alpha}}. \quad (6)$$

For very massive black holes the critical radius becomes

² The parameter n_0 can be substituted by $n_0 = n_c r_H^{-\alpha}$ into the more common number density n_c at the influence radius r_H .

³ We replace $v(r) \propto \frac{r}{t_{cross}}$.

larger than the influence radius of the black hole and Eq. 4 must be modified according to Frank & Rees (1976):

$$r_{crit} \propto (r_{cap} r_H n_0)^{-\frac{1}{1+\alpha}}. \quad (7)$$

We assume the velocity dispersion to be $\sigma^2 \propto \frac{GM(r)}{r} \propto G n_0 M_\star r^{2+\alpha}$ and use the same formalism (Eq. 5) to derive Eq. 7. The capture rate for $r_{crit} > r_H$ becomes:

$$\dot{C} \propto r_{cap} r_H n_0^{\frac{3}{2}} G^{\frac{1}{2}} M_\star^{\frac{1}{2}} (r_{cap} r_H n_0)^{-\frac{2+3\alpha}{2(1+\alpha)}}. \quad (8)$$

For simplicity we adopt the number density profile to be $n(r \leq r_{crit}) = n_0 r^\alpha$ and thus assume α to remain constant. Real galactic nuclei with SMBHs more massive than $10^7 M_\odot$ can deviate from pure power law profiles at radii $r \leq r_{crit}$, whereas the inner density profiles of large elliptical galaxies are nevertheless well approximated by simple power law profiles (Trujillo et al. 2004). Eq. 8 is valid for $-3 < \alpha < -1$.

These equations which are derived from the very general angular momentum diffusion concept of Frank & Rees (1976), will lose their applicability for systems where the stellar phase space is not well-occupied with sufficient amounts of low angular momentum stars. Gaps in the phase space distribution, for example carved out by binary-SMBH evolution must first be repopulated, whereas the relaxation driven refilling process may take longer than one Hubble time H_0^{-1} for large elliptical galaxies. Hence for these systems the two-body relaxation driven capture rate will be strongly suppressed (Merritt & Wang 2005).

3 DESCRIPTION OF THE N-BODY MODELS

In the following sections the computations and results will be specified. We make use of conventional N-body units (Heggie & Mathieu 1986). For readers being unexperienced with these units, a very short overview is given below.

3.1 N-body units

The set of N-body units is defined by

$$G = M = 1 \quad (9)$$

where G is the gravitational constant and M the total mass. If the system is gravitationally bound and in virial equilibrium with $r_{vir} = 1$ then the total energy E , which is the sum of the kinetic and potential energies of all particles, is $E = -\frac{1}{4}$. N-body timescales which are used as the time base for the computations are defined to be $\frac{t_{cross}}{2\sqrt{2}}$. Here $t_{cross} = \frac{2r}{\sigma}$ is the crossing time of the particles at $r = r_{vir}$. The half mass i.e. half light radius r_e for a constant $\frac{M}{L}$ -ratio is usually scaled to equal $r_e = r_{vir} = 1$. It is of the order of kpc scales in physical units for real elliptical galaxies. For example one N-body timescale would correspond to $t = 7 \cdot 10^6$ yr in physical units for a spherical bulge or galaxy of Sérsic type (n=4, see § 3.2) with a half light radius $r_e \approx 0.65$ kpc and total stellar mass $M = 10^9 M_\odot$. In § 6.1 and Appendix B the detailed procedure how the computational results are transformed from N-body to physical units is given.

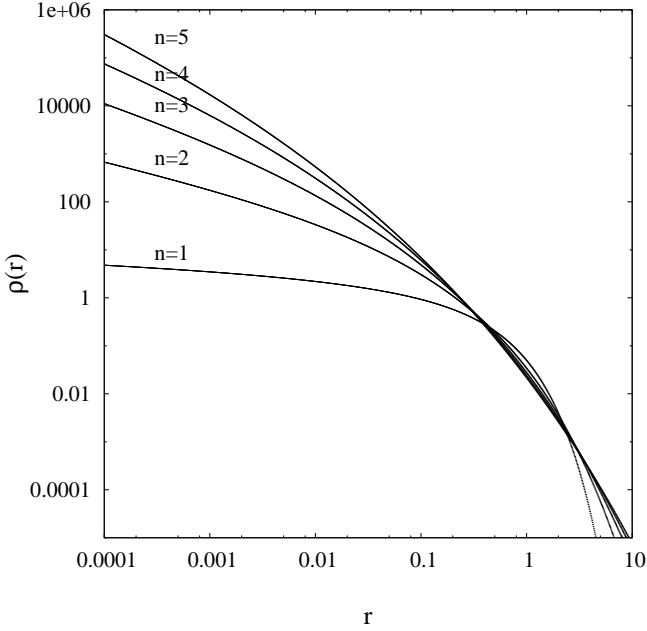


Figure 1. Scale-free density profiles of different Sérsic models.

3.2 Generation of the models

The observed surface brightness profiles $I_n(r)$ of bulges and elliptical galaxies are well approximated by the following Sérsic law (Sérsic 1968; Caon et al. 1993):

$$I_n(r) = I_e \exp \left\{ -b_n \left[\left(\frac{r}{r_e} \right)^{\frac{1}{n}} - 1 \right] \right\}. \quad (10)$$

Here n is the Sérsic index. It represents the strength of light concentration towards the center. The parameter $I_e = I(r_e)$ specifies the surface brightness at the corresponding half light radius r_e , whereas b_n is a scaling factor (Ciotti & Bertin 1999). The 2D density profile can also be reconstructed from the measured surface brightness profile using an appropriate mass-to-light ratio, which for our purposes is assumed to be constant along the radial distance to the center of the galaxy.

In order to study the environmental impacts of massive black holes, an unaltered and original Sérsic density profile is chosen for the initial state of the models. These N-body models are set up using the same method as described in Hilker et al. (2007). First the 2D Sérsic models are deprojected into 3D density distributions using Abel's integral equation. From the 3D density profile $\rho(r)$, the potential, $\phi(r)$, and mean mass within radius r , $M(< r)$, can be deduced. For a non-rotating, spherical system with an isotropic velocity distribution, the distribution function $f(H)$ is ergodic, where H is the Hamiltonian i.e. the total energy of the system. The radial velocity distribution is then derived from $f(H)$ by using eq. 4.46a from Binney & Tremaine (2008). The actual positions as well as velocities of the N-body particles are distributed correspondingly in 3D. The program is modified by adding a $1/r$ -potential of the black hole of mass $M_\bullet = 0.01$ in

N-body units (Heggie & Mathieu 1986)⁴. This step is necessary because otherwise the velocities of particles close to the black hole in the N-body computations would be too low and the system out of equilibrium. The cut off radius for the models is chosen to be 20 times the half light/mass radius.

3.3 NBODY6 numerical dynamics software

The up to date version of NBODY6 (Aarseth 1999, 2003) with Graphical Processing Unit (GPU) support is used for the direct N-body integrations. A black hole is added by a SMBH particle of mass $M_\bullet = 0.01$. It is implemented into the models at the center of mass while being initially at rest. Particles which fall below the limit of the capture radius $r_{\text{cap}}^{\text{sim}}$ are removed from the simulations while their masses are added to the SMBH particle. The capture radius $r_{\text{cap}}^{\text{sim}}$ remains constant⁵. To ensure correct dynamics, the SMBH particle receives the center of mass velocity after the capture event.

3.4 The need for a large set of simulations

In order to extrapolate many scale-free models to astrophysical systems which contain some orders of magnitudes more stars than are possible to be simulated with direct N-body integration methods on modern GPUs, the relaxation driven effects in angular momentum and energy space as well as every other N dependent systematic effect (see § 5.1 & § 5.2) must be determined. This can be achieved by simulating models with different numbers of particles but otherwise identical physical parameters. In doing so several particle models following a Sérsic $n = 4$ density profile are generated. It is desirable to simulate these models for as many different black hole configurations as possible in order to use the formalism in § 6.1 for the extrapolation to the black hole of interest, hence increasing the computational effort considerably. The masses of the particles $m_i = N^{-1}$ are always scaled to ensure $\sum_i m_i = 1$ in N-body units (Heggie & Mathieu 1986). $N=15 \times 1 \text{ k}$, $15 \times 2 \text{ k}$, $10 \times 5 \text{ k}$, $5 \times 10 \text{ k}$, $5 \times 25 \text{ k}$, $2 \times 50 \text{ k}$, $2 \times 75 \text{ k}$ and one model containing each 100 k, 150 k, 250 k and 500 k particles are generated and simulated. All these models are simulated forward in time up to $\frac{100}{2\sqrt{2}}$ crossing times at the virial radius $r_{\text{vir}} = 1$ i.e. 100 N-body timescales for three different black hole capture radii $r_{\text{cap}}^{\text{sim}} = 2, 4, 8 \cdot 10^{-7}$. Energy values and relative energy errors $|\Delta E| = \left| \frac{E(t_n) - E(t_{n-1})}{E(t_{n-1})} \right|$ are evaluated directly

⁴ The differences between a $1/r$ -potential and a realistic Schwarzschild or Kerr black hole potential are completely insignificant for distances of several hundred r_{cap} away from the black hole. This is typically the distance where the innermost particles are located.

⁵ In reality the capture radius would change as well as the total number of capture events. However in order to simplify our extrapolation formalism to realistic galaxies and due to the fact that the mass gain of the black hole within $T = 100$ NBODY timescales is limited to the order of a few percent, it is assumed to be constant.

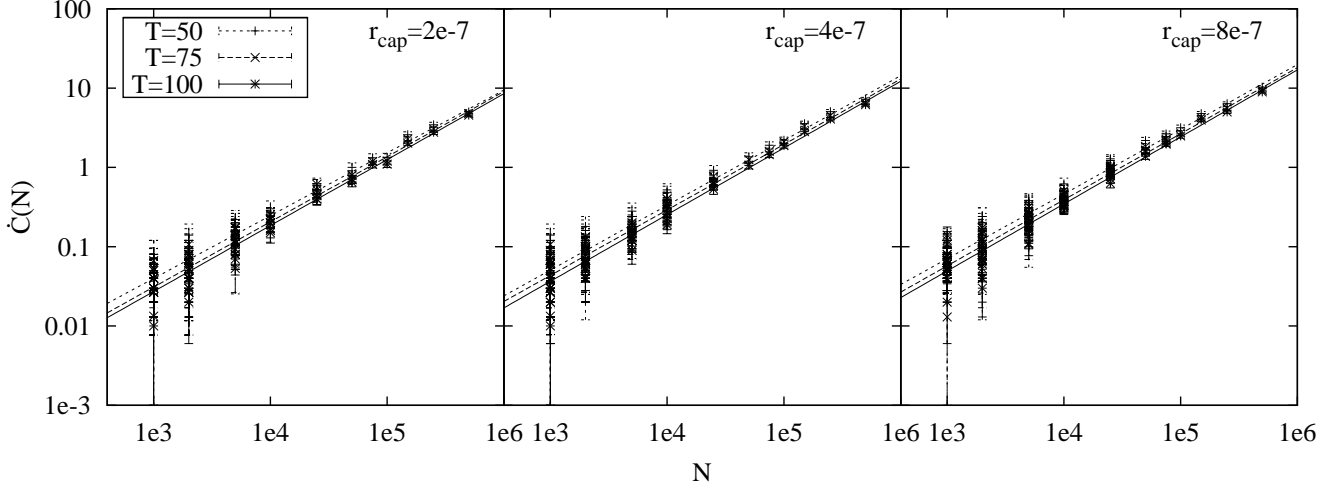


Figure 2. The capture rates per one N-body time unit for the three different black hole capture radii, evaluated from the total amount of swallowed particles within the timespan of $T = 50, 75$ & 100 N-body time units. These values are best fitted by the power law function $\dot{C}(N) = aN^b$, here N refers to the total number of simulated particles.

with the NBODY6 software and controlled every new N-body timescale. The relative energy errors usually not exceeded values of $|\Delta E| = 10^{-8} - 10^{-4}$. A few models had to be discarded afterwards as they suffered from repetitive energy errors in excess of $|\Delta E| = 10^{-2}$. To guarantee unbiased capture rates we also discarded models in which the position of the black hole was offset by a distance $d \geq 0.1$ from the density center of the particle distribution. The statistical significance of the numerous low N models is increased by simulating as many models as possible. The required time for the computations of all simulations exceeds a timespan of seven months on five modern GPUs.

4 RESULTS

In Fig. 2 the number of particles being swallowed by the black hole is plotted against the total number of particles. This is done for each black hole capture radius $r_{\text{cap}}^{\text{sim}} = 2, 4, 8 \cdot 10^{-7}$. Moreover the total number of captured particles within $T = 50, 75, 100$ N-body integration times is divided by these values to obtain the capture rate per N-body timescale. The number of captures averaged over all runs are then approximated by a power law function

$$\dot{C}(N) = aN^b \quad (11)$$

with the help of the *Marquardt-Levenberg* minimization method and independently by a grid scanning algorithm minimizing the Chi-square error statistics. The free parameters a and b have to be positive real numbers while the boundary condition $\dot{C}(N)|_{N=0} = 0$ requires no offset. To reduce the correlation between the parameters a and b to zero, we normalize the power law function $\dot{C}(N) = a'(N/\bar{N}_L)^b$ during fitting. The denominator \bar{N}_L refers to the logarithmic mean. The resulting effect can be seen in Fig. 3. These uncorrelated values⁶ are used for

the extrapolation to realistic values. The justification for using a power law approximation for the capture rate $\dot{C}(N)$ from the simulations comes from Eq. 6 when replacing $n_0 = N\rho_0$ and $M_* = N^{-1}$. Poisson square root errors $\sqrt{N_c}$ are assumed for all values and N_c is the total number of captured particles. The results can be found in Table 1. Additionally the reduced Chi-Square values χ_μ and the χ^2 -probability function $Q(\mu, \chi^2)$ are calculated in order to test the validity of a power law approximation for the capture rate. Given the values in Table 1, the hypothesis of a power law function seems to be a reasonable assumption. However, for the determination of the error values of parameters a, b the square root errors $\sqrt{N_c}$ are rescaled slightly by the values $\sqrt{\chi_\mu}$ from Table 1 to obtain $\chi_\mu = 1$. Otherwise the quoted error values would be underestimated for the case of $\chi_\mu \geq 1$ (Press et al. 1992)⁷.

The advantage of numerical simulations over analytical expressions like Eq. 6 are given in the ability to take dynamical aspects like cusp formation, dynamical heating (§ 5.1) and a wandering SMBHs (§ 5.2) into account. These depend strongly on time and on the total number of particles and may influence the capture rate $\dot{C}(N)$. The predicted power-law index of Eq. 6 is therefore not expected to exactly match the value obtained from the simulations. In fact Eq. 6 would only predict $\dot{C}(N) \propto N^{\frac{4.5+2\alpha}{4+\alpha}} \approx N^{0.6}$ for $\alpha \approx -1.5$ compared to $\dot{C}(N) \propto N^{0.83}$ from the computations. The difference is caused by stronger dynamical evolution and cluster heating in low number particle simulations accompanied by a decrease in the total number of particles falling into the black hole. Models containing many more particles have much smoother potentials and relaxation driven effects (notably cluster heating) need longer to influence (decrease) the capture rate (Fig. 4). Consequently the exponent b of the power law function which approximates the number of

⁶ To simplify the extrapolation formalism, the renormalized constant of proportionality a' and its error is afterwards transformed

back to $a = \frac{a'}{\bar{N}_L^b}$. This does not affect the correlation coefficient $\rho = 0$ between a, b .

⁷ Chapter 15.1

T	$r_{\text{cap}}^{\text{sim}}$	$a(10^{-5})$	b	χ_{μ}	Q
50	$2 \cdot 10^{-7}$	16.76 ± 3.11	0.792 ± 0.018	0.82	0.792
	$4 \cdot 10^{-7}$	17.95 ± 2.89	0.817 ± 0.014	1.06	0.359
	$8 \cdot 10^{-7}$	25.08 ± 3.92	0.816 ± 0.014	1.41	0.024
75	$2 \cdot 10^{-7}$	10.63 ± 1.95	0.822 ± 0.016	1.01	0.450
	$4 \cdot 10^{-7}$	14.46 ± 2.09	0.826 ± 0.013	1.13	0.245
	$8 \cdot 10^{-7}$	18.15 ± 2.51	0.833 ± 0.012	1.41	0.022
100	$2 \cdot 10^{-7}$	8.73 ± 1.33	0.831 ± 0.013	0.83	0.788
	$4 \cdot 10^{-7}$	10.98 ± 1.49	0.841 ± 0.012	1.12	0.255
	$8 \cdot 10^{-7}$	14.41 ± 1.97	0.845 ± 0.012	1.57	0.005

Table 1. Fit parameters of the power law approximation (Eq. 11) for the simulated Sérsic $n = 4$ models. The black hole capture radii and timescales T are given in N-body units. $\chi_{\mu} = \chi^2/\mu$ corresponds to the reduced Chi-Square values, μ are the degrees of freedom and $Q = \Gamma(0.5\mu, 0.5\chi^2)$ the χ^2 -probability function which estimates the likelihood of the power law fit.

captured particles of the total set of simulations becomes larger than expected from Eq. 6. These dynamical processes are reflected by the values of a, b at different timescales. The constant of proportionality a decreases in time, whereas the slope parameter b is consistent with a small increase from $b \approx 0.80$ at time $T = 50$ up to $b \approx 0.83$ at time $T = 75$. Thus the exponent of the power law function which approximates the capture rates becomes slightly larger, whereas the constant of proportionality decreases. Moreover the $T = 50$ values may still be influenced by initial conditions. There are minor changes in b from $T = 75$ to $T = 100$.

For the purpose of this study the rate \dot{C} is assumed, within the statistical uncertainty, to remain unchanged when extrapolated to larger values of N . This assumption can only hold if the phase space is already well occupied with sufficient amounts of low angular momentum stars. This is a necessary condition for the steady diffusion process of stars into the loss cone. The capture rates of the Sérsic $n = 4$ models are found to be maximal at the beginning of the simulations in contrast to Sérsic $n = 2$ models with their much shallower density profiles (Fig. 4). This demonstrates the above assumption to be credible, at least for galactic nuclei containing SMBHs less massive than $10^7 M_{\odot}$. In such galaxies the diffusively refill of any small gap with radius $r_{\text{gap}} \ll r_H$ would anyway occur on a timescale shorter than a Hubble time (Merritt 2005). The observed strong N dependence ($b=0.83$) may become irrelevant or absent for black holes more massive than $10^7 M_{\odot}$, especially if they have core profiles. For these systems the loss cone refilling timescale $T_{\text{refill}} \approx \theta_{\text{lc}}^2 T_{\text{rel}}$, becomes very long. Once the initially filled loss cone becomes emptied within a few crossing times, the capture rate \dot{C} would stagnate at insignificant values as long as there is no re-population mechanism more efficient than angular momentum diffusion (Merritt & Wang 2005; Merritt 2005).

This effect can be illustrated by simulating Sérsic $n = 2$ models. These have a slower dynamical evolution, a different cusp and cluster heating timescale and a reduced population of low angular momentum stars compared to the Sérsic $n = 4$ models. In this way, qualitative limitations

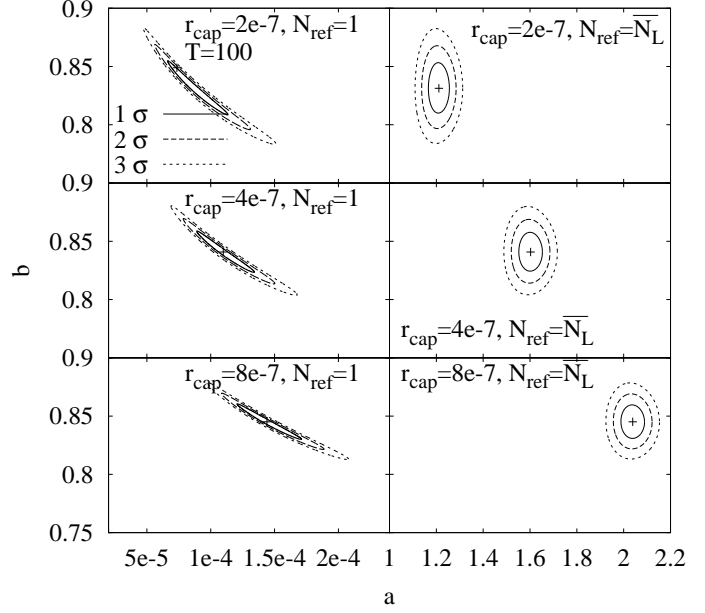


Figure 3. The error ellipses for the models after $T = 100$ before (left) and after (right) renormalization. The shape of the error ellipses becomes nearly circular which proves the parameters to be uncorrelated.

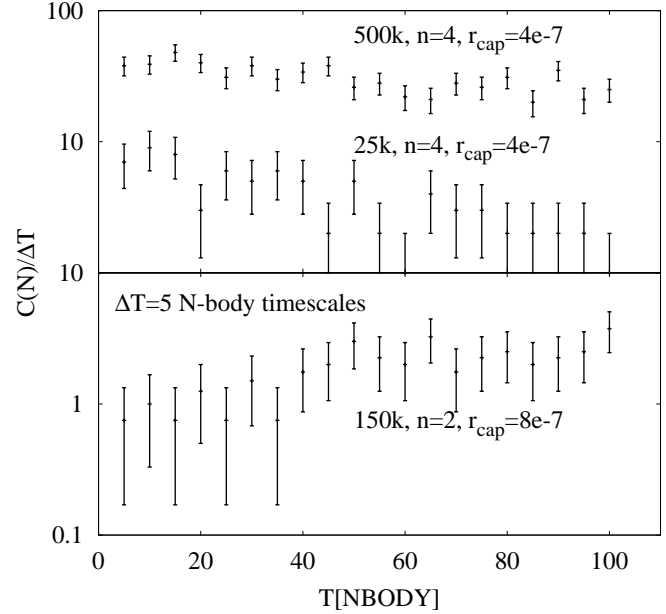


Figure 4. Time evolution of the capture rates for Sérsic $n = 4$ & $n = 2$ models. The statistical significance of the latter ones is increased by averaging over three simulations.

on the number of capture events for core-type galaxies with shallow central density profiles (Fig. 1) can be obtained. Even though the extended outer profiles of the most-massive elliptical galaxies are conform with a large Sérsic index n , the 'depleted' core-type central regions (this is where the relevant black hole physics take place) are more similar in their appearance to the shallow centers

of low n models⁸. A strongly reduced disruption rate in comparison to the Sérsic $n = 4$ models is evident in these computations. The enlarged radius of influence r_H and therefore the difference in the extrapolation formalism to realistic galaxies can not compensate these differences. Moreover in the largest simulated Sérsic $n = 2$ models, the capture rate stagnate first around insignificant values. It starts increasing (Fig. 4) afterwards, accompanied by the relaxation driven formation of a cusp and a population of stars with sufficiently low angular momentum. If we assume this behaviour to persist unchanged up to even larger numbers of particles, i.e. to large core-type galaxies where no cusps can form on timescales shorter than H_0^{-1} , these numerical findings confirm analytical predictions (Wang & Merritt 2004) in a qualitative way. The capture rate of stars in large core-type galaxies is very low, as long as the diffusive refill of the angular momentum space with a sufficient number of stars, i.e. the cusp formation timescale, takes longer than a Hubble time. See also § 7 & Appendix C for more details on this topic.

Finally the here performed simulations of the Sérsic $n = 4$ models strongly support the scenario of Frank & Rees (1976) in which stars are driven into SMBHs via diffusion in angular momentum space and not only by diffusion in energy space. From the most elementary considerations of energy diffusion and by assuming the two-body relaxation time to be $T_{\text{rel}} \propto \frac{N}{\ln(N)}$, one would expect $\dot{C}(N) = \frac{dN}{dt} \propto N \cdot T_{\text{rel}}^{-1} \propto \ln(N)$. Such a small increase of the capture rate with N is incompatible with our results.

5 DYNAMICS & SCALING ISSUES

The capture rate is influenced by several dynamical processes which are described below.

5.1 Cusp formation and cluster expansion

The process of relaxation strongly influences the dynamics of stars around a SMBH. In Bahcall & Wolf (1976) the relaxation driven evolution of the stellar density profile near a SMBH is determined. It is found that the energy which some stars loose through near encounters is balanced by an outgoing flux of energy if the slope of the density profile is $\alpha = -1.75$. The required time to form such an equilibrium density B&W profile strongly depends on the relaxation time which becomes larger the smoother a gravitational potential is (Spitzer 1987).

The $\alpha = -1.75$ profile is compatible with the present N -body models only up to $N = 25 - 50$ k where relaxation is

⁸ This is also one reason which complicates the discrimination between 'true' cores, formed by the dynamical evolution of massive binary black holes and those in which only the outer envelopes are modified by near encounters. In the latter case the outer profile extrapolated to inwards radii would suggest the existence of a core (Hopkins & Hernquist 2010). The binary black hole mechanism may also be accompanied by other processes lowering the central stellar density (Merritt & Vasiliev 2010; Schawinski et al. 2006).

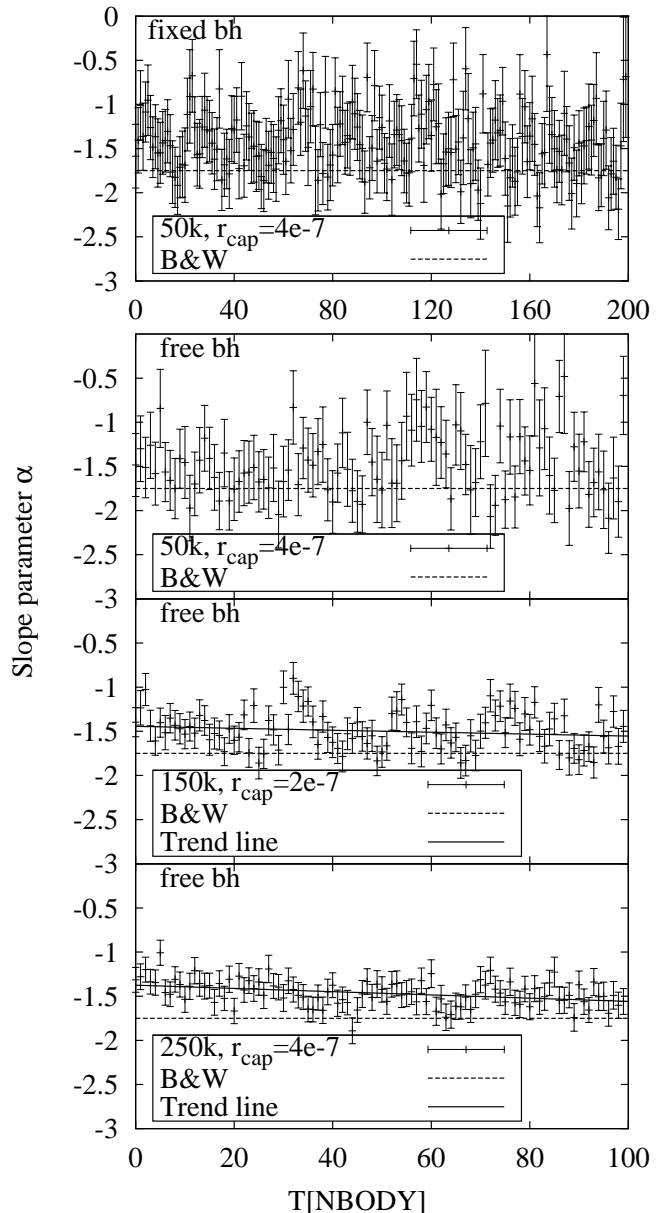


Figure 5. Time evolution of the central slope parameter α plotted for the 50 k, 150 k and 250 k models. The linear trend (solid line) is only drawn for the 150 k and 250 k models, while the first one (fixed black hole) was simulated forward in time up to $T = 200$.

strongest and the statistical scatter is large. The $N > 50$ k models, which allow a more precise measurement of α , are found to be in the developing stage towards more cuspy profiles. In Fig. 5 the time dependent central slope parameter α within $r = 0.004$ is plotted for some models. The radius r is chosen to be 20% smaller than the time and model-averaged black hole influence radius⁹ in order to ensure that the slope parameter is not determined for radii larger than r_H at the beginning of the simulation when the mass and

⁹ See Appendix B for information regarding the determination of r_H .

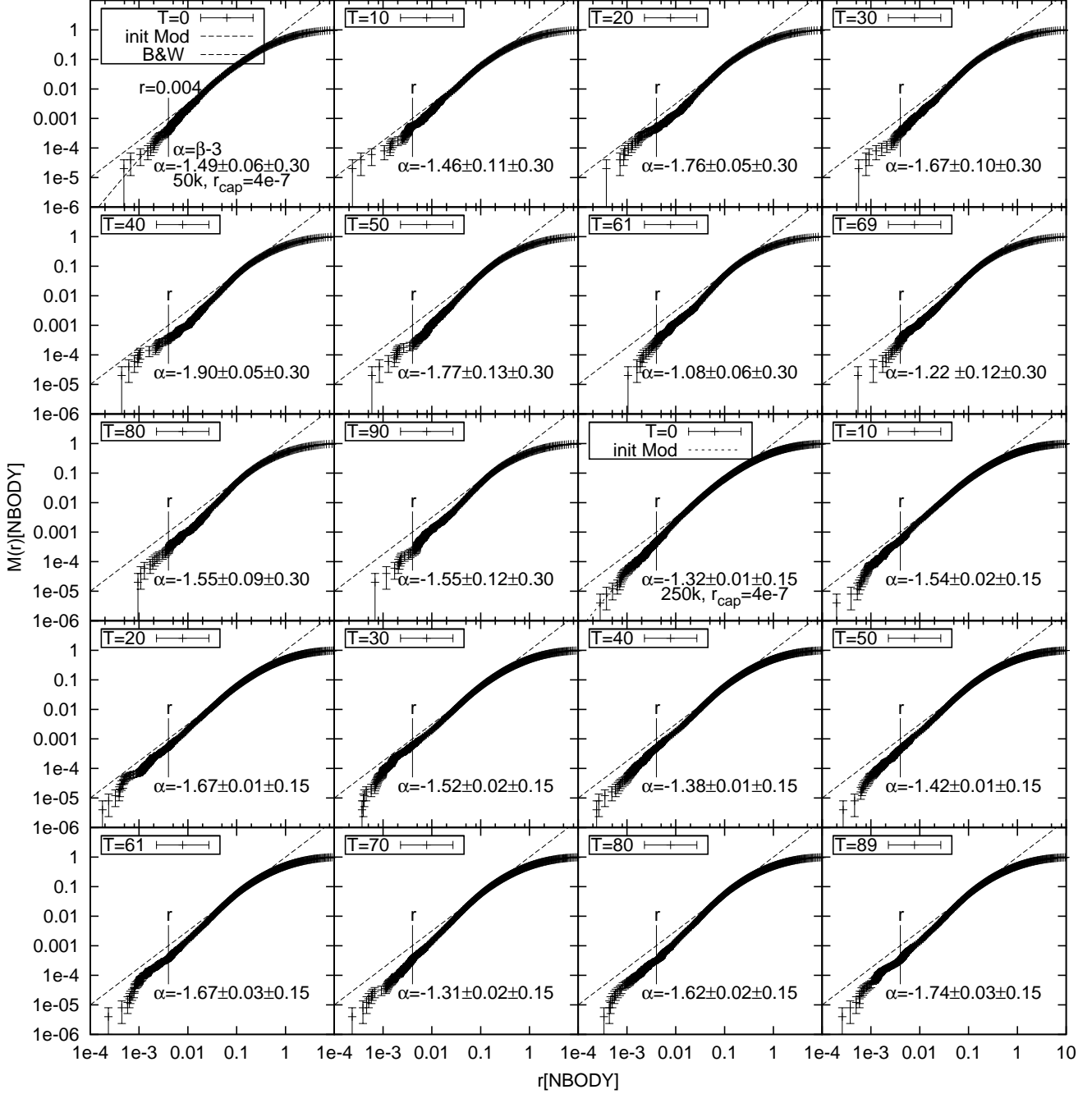


Figure 6. Mass profiles of two models. The thin dashed black line represents the gradient of the B&W profile while the thick dashed black line (only drawn for $T=0$) displays the unaltered Sérsic $n = 4$ model. The first error on α corresponds to the fitting error while the second one to the statistical error inferred from Monte Carlo simulations. The profiles and thus α are evaluated for radii $r \leq 0.004$. For more informations see the text below.

influence radius of the black hole is smallest. In order to obtain the central slope parameter α , it is inappropriate to calculate the density profile $\rho(r) \propto r^\alpha$ from given shells of thickness Δr and densities $\rho(r + \Delta r)$. Unfilled shells, especially in low N models, would strongly bias the determination. In order to circumvent this difficulty, the cumulative mass function $M(r) \propto r^\beta \propto \int_0^r r'^2 \rho_0 r'^\alpha dr'$ is calculated and the density slope parameter $\alpha = \beta - 3$ (equating coeffi-

cients) is determined from the measured β . This approach is tested by Monte-Carlo simulations in which several thousand models of particles following a $\rho \propto r^{-1.75}$ distribution are realized. For each of these models the central slope parameter α within $r = 0.004$ is calculated. The models are scaled such that the number of particles within $r = 0.004$ is equal (within the statistical scatter) to those of the 25 k, 50 k, 75 k, 150 k and 250 k simulations. The standard devi-

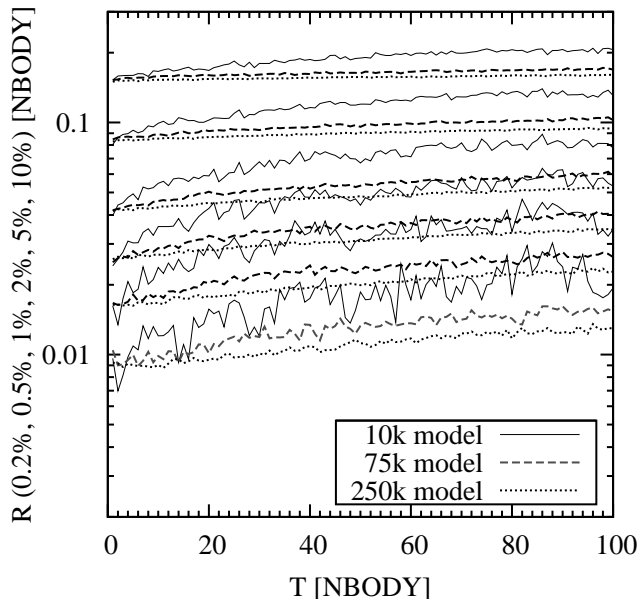


Figure 7. A comparison between the time evolution of several Lagrange radii for three different simulated models. As expected from theory, the Lagrange radii evolve faster to larger values in simulations containing fewer particles. The fluctuations are statistical in nature. The position of the black hole is used as the reference center.

ation σ from the obtained normal distribution¹⁰ of central slope parameters is then taken as a reasonable estimate for the statistical error in addition to the one obtained from the fit itself. In Fig. 6 the time evolution of the mass profiles of two models are plotted.

In order to estimate the dependence of a wandering black hole on cusp formation processes and finally the capture rate, simulations of fixed black holes are desirable. Such simulations are realized by making use of a modified NBODY1 code (see §5.3 for more details regarding the capture rates). Within the large statistical errors, no significant difference in the density profiles between the free floating and fixed black hole is identified for the 50 k model. This is not an unexpected finding since the most bound particles, which are also the particles with the highest probability of being captured, are expected to follow the motion of the black hole. However a rigorous statistical evaluation is beyond the scope of this study.

While the capture rate is increased by cusp formation, dynamical heating counteracts by reducing the central density. The cluster starts to expand by decreasing the absolute value of its binding energy due to increasingly more strongly bound particles which are losing energy by

¹⁰ Actually very small particle numbers within $r = 0.004$ bias the power-law density-approximation and the distribution of central slope parameters becomes asymmetric with a tail towards very large values. This may partially account for some extreme outliers especially in low N models, whereas for larger models the distribution becomes more symmetric and the expectation values μ center around $\alpha = -1.75$.

relaxation. These particles, which may finally be swallowed by the black hole, are transferring their kinetic energy to other particles. This heating is illustrated by the time evolution of the Lagrange radii (Fig. 7). As a consequence the capture rate is expected to depend strongly on the density profile close to the black hole (Eq. 6).

In reality mass segregation of heavier bodies being relevant for multi-mass systems (Alexander & Hopman 2009; Baumgardt et al. 2004b; Morris 1993; Preto & Amaro-Seoane 2010), stellar collisions (Bailey & Davies 1999; Dale et al. 2009), a significant fraction of primordial binary stars (Hopman 2009), torques from anisotropic matter distributions acting as massive perturbers (Perets et al. 2007), star formation by gas inflow (Hopkins & Quataert 2010) and the possible presence of IMBHs (Baumgardt et al. 2006) would complicate the dynamics of stars close to a SMBH even more. These effects are also expected to accelerate the dynamical evolution and to enhance the number of stellar disruption events. Newly formed stars may replace those lost by tidal disruptions while tidal torques from IMBHs or a second SMBH are expected to refill the loss cone efficiently. Recoiled black holes should also enforce a burst of stellar disruptions (Stone & Loeb 2010). In nature the relaxation driven B&W cusp formation takes very long and is expected to exceed one Hubble time H_0^{-1} for black hole masses larger than $10^7 M_\odot$ (Freitag et al. 2008).

5.2 Wandering black hole

In the simulations the SMBH particle responds to the interaction with other particles which causes the SMBH to wander. This might affect the formation of a density cusp and influence the capture rate (Baumgardt et al. 2004a). Chatterjee et al. (2002) gives a very detailed overview of the relevant forces acting on a SMBH. They are summarized below.

The here performed simulations differ only in two ways from the N-body simulations done by Chatterjee et al. (2002). The black hole is allowed to swallow particles and the forces are unsoftened. The SMBH moves around the common center of mass due to the gravitational interaction with particles bound to it, whereas unbound particles are forcing the black hole to wander in a way which resembles the Brownian motion of molecules. The latter process is the dominant contribution to the wandering of the black hole (see Fig. 8).

The situation is now complicated by the possible occurrence of violent three body encounters, e.g the interaction between the black hole, a strongly bound particle in orbit around it and another one. Recoil events force the black hole and its surrounding particles to move outwards. The mass fraction, $\frac{m}{M_\bullet}$, is usually orders of magnitudes larger in any performed N-body simulation than it is in a realistic nucleus of a galaxy. And, because the recoil effect becomes stronger for a larger fraction $\frac{m}{M_\bullet}$ and for smaller capture radii $r_{\text{cap}}^{\text{sim}}$, wandering of the SMBH in the

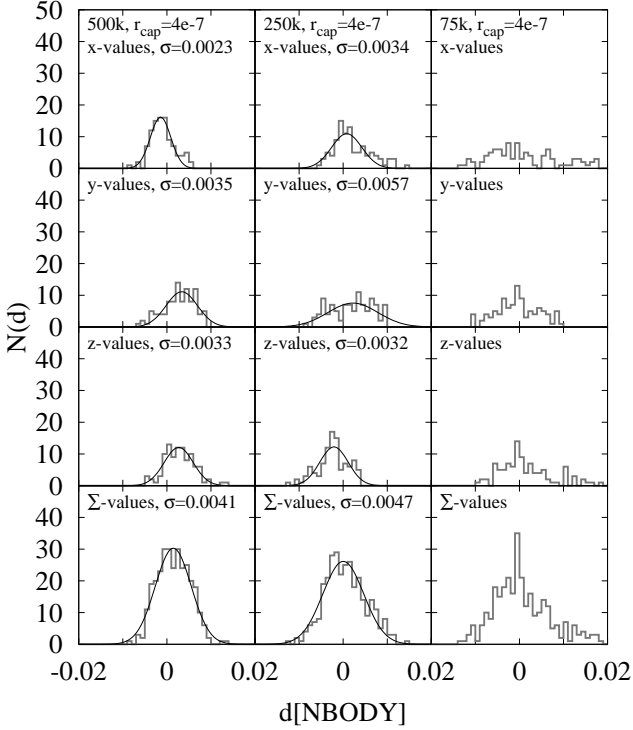


Figure 8. The 100 binned ($\Delta d = 0.001$) x, y, z-positions of the SMBH particle with a capture radius $r_{\text{cap}}^{\text{sim}} = 4 \cdot 10^{-7}$ for the 500k, 250k and 75k model. In the last row the sum of these values is plotted and approximated by a normal distribution. The probability distributions are well approximated by a Gaussian underlining the character of the Brownian motion. The relevant length scale d is given in units of the virial radius $r_{\text{vir}} = r_e = 1$. The SMBH particle in the 75k model experienced a minor kick during the integrations.

N-body models is expected to modify the processes leading to the formation of a cusp. Consequently, the simulated capture rate may become affected. If the recoil kick of the SMBH particle is strong enough to eject it out of the density center or even from the whole cluster, the capture rate would drop significantly. This is expected, due to obvious reasons, to happen more likely in simulations with low particle numbers. As a consequence the extrapolated N-dependent capture rate would be strongly biased and the best fitted slope parameter, b , may be too large. Therefore the actual position of the SMBH particle is compared to the density center of the matter distribution for every simulated model and at every new N-body time unit. The black hole particle is not considered in the calculation of the density center which is determined by the method described in Casertano & Hut (1985). If the position of the black hole and the density center are offset from each other by $d = 0.1$ in N-body units, the simulation is removed and replaced by a different one. In nearly all simulations this offset is smaller than $10^{-3} - 10^{-2}$. This guarantees that the results are not biased by displaced black holes in the low N models.

But even by removing those few models where "unnatural" kicks and displaced black holes are observed, the wandering of the black hole itself might affect the capture rate. The wandering radius can be determined by the

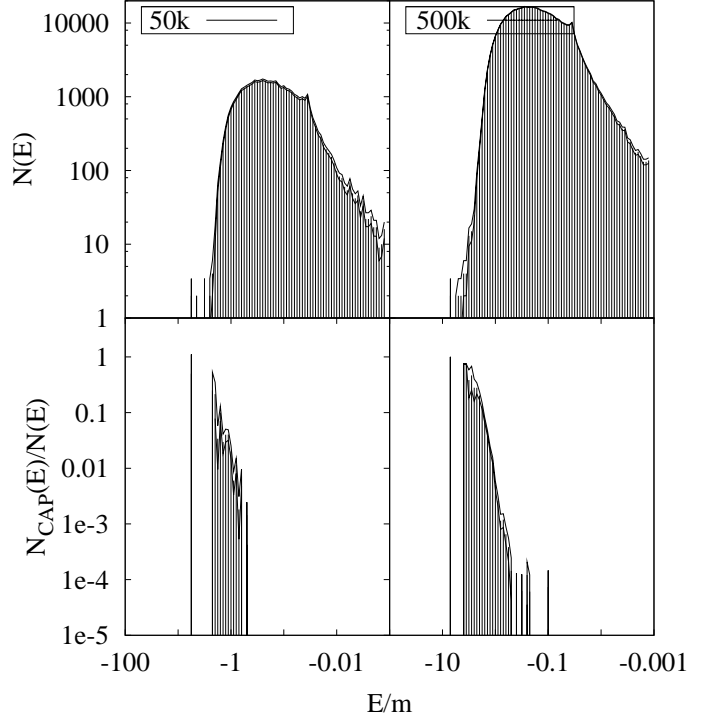


Figure 9. In the upper two figures the binned specific energy $\frac{E}{m}$ distributions of the 50k, $r_{\text{cap}}^{\text{sim}} = 4 \cdot 10^{-7}$ and 500k, $r_{\text{cap}}^{\text{sim}} = 4 \cdot 10^{-7}$ models are plotted. The lower diagrams depict the ratio of captured particles to total number of particles within the given energy bins. Evidently only the particles with the most negative energy i.e., the most strongly bound particles are accreted as expected from theory. The upper and lower (black) lines represent the error uncertainties.

standard deviation of the normal distribution (Fig. 8). It is found to be comparable in size to the influence radius $r_H = 0.005$ (for the 250k model) and becomes gradually smaller for larger particle numbers i.e. smaller mass fractions $\frac{m}{M_\bullet}$.

A first clue about the degree to which the wandering black hole affects the results can be obtained by a closer look at the energies of accreted particles. If only particles are swallowed which are strongly bound i.e. have the most negative energies, the effect of Brownian motion on the capture rate is expected to be rather small, since the cloud of strongly bound particles moves together with the black hole. In Fig. 9 the initial energy distribution for two models is shown. Also plotted is the fraction of the accreted particles to the total number of particles within a given energy bin. Evidently only the most strongly bound particles are captured. If the energy $E = -\frac{M_\bullet m}{r} + 0.5mv_m^2 + 0.5M_\bullet v_M^2$ of the particle of mass m and black hole is negative, shortly before it enters the capture radius and is removed, the particle is gravitationally bound to the SMBH. In our models the vast majority of particles are gravitationally bound to the black hole, e.g. the fraction of bound particles centers around 100% in the low-N models and 85 - 95% in the largest-N models.

We therefore conclude that a wandering black hole

does not bias the capture rate in a way that would make it unrealistic when extrapolated to real IMBHs and SMBHs. The performed simulations automatically contain the gradual change in the number of accreted particles which are influenced by the wandering of the black hole. Our largest N-computations already approach realistic IMBHs embedded in globular clusters. To resolve all doubts that the steep dependence on N of the capture rate, $\dot{C} \propto N^{0.83}$, is not caused by the systematics of the wandering black hole, especially in low N models, direct N-body simulations with fixed black holes (§ 5.3) are performed. For completeness it should also be mentioned that the N-body models include two additional effects: (i) A restoring force which arises between the black hole and the overall potential of the stellar distribution, especially if it has a cuspy density center, and (ii) a dynamical frictional force when the black hole passes through the cloud of particles (Chandrasekhar 1943a,b,c; Chatterjee et al. 2002).

5.3 Fixed black hole

Simulations with a fixed black holes are realized by using NBODY1. Unfortunately it is impossible in NBODY6 to fix the SMBH particle to a specific location while simultaneously using all of its computational benefits. On the other hand the usage of an independent N-body software implementation reduces the possibility of systematic errors. The NBODY1 simulations are performed on special-purpose, GRAPE-6A boards (Fukushige et al. 2005) at the stellar Populations and Dynamics Research Group in Bonn. The black hole is mimicked by an (unsoftened) external $\frac{1}{r}$ potential which is directly implemented into the code. Particles which cross the capture radius are removed, while their masses are added to the mass of the black hole. To circumvent collisions between field particles, a small softening parameter $\epsilon = 10^{-4}$ is used. Additionally some strongly bound particles around the external potential are erased artificially (the number corresponds to roughly 30% of the total number of "true" capture events) in order to prevent gradual slow downs, large energy errors and/or the complete crash of the simulations. The energies of all removed particles are handled carefully to ensure a correct energy output. Due to these limitations and the much smaller sample of simulated models, the NBODY1 computations are not used for the extrapolation to realistic galaxies but only for a rough comparison to the much more advanced NBODY6 simulations. In Fig. 10 the results are plotted. Despite the large simplifications of the NBODY1 computations, the power law index b of the capture rate, $\dot{C} \propto N^b$, agrees, within the statistical uncertainties, closely with the index obtained with the much more sophisticated NBODY6 simulations with free moving SMBHs. As a consequence a (strongly) wandering black hole does not bias the low N results in a way which would be dangerous when extrapolating these to astrophysical systems harboring many more stars than particles in our simulations. Of course this behaviour may change for initial black hole masses different from the one $M_\bullet(t=0) = 0.01$ used in these computations.

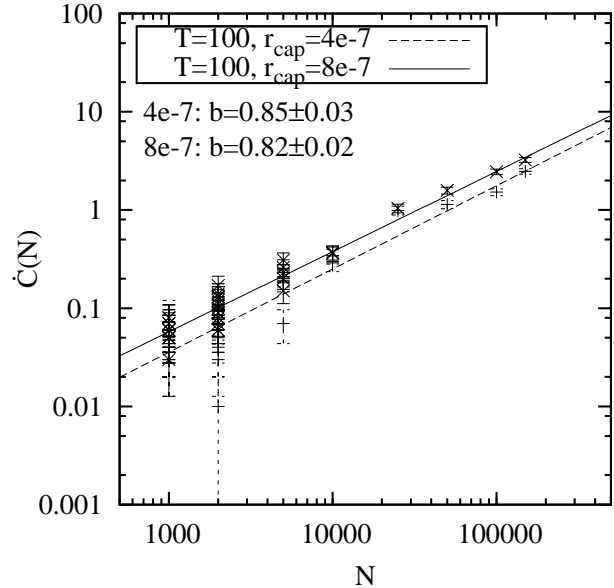


Figure 10. Results of the simulations with a fixed black hole. Strongly bound particles which needed to be removed artificially to prevent slow downs or a computational crash are not considered in the evaluation of the slope. Note the excellent agreement with the results obtained for the more realistic NBODY6 computations (Fig. 2).

6 DISCUSSION

6.1 Scaling to realistic galaxies

The so-far presented results must be scaled to astrophysical systems in order to infer the rates at which stars are disrupted by central, supermassive black holes. From the following relation

$$\left. \frac{r_{\text{cap}}}{r_H} \right|_{\text{sim}} = \left. \frac{r_{\text{cap}}}{r_H} \right|_{\text{astro}}, \quad (12)$$

which must be necessarily fulfilled, the capture radii, r_{cap} , for the corresponding black holes of interest must be determined. In order to scale to astrophysical systems, we use the $M_\bullet - \sigma$ relation from Schulze & Gebhardt (2011),

$$\left(\frac{M_\bullet}{M_8} \right) = 1.51 \left(\frac{\sigma}{200 \text{ km s}^{-1}} \right)^{4.32}, \quad (13)$$

and the expression for the radius of influence,

$$r_H = \frac{GM_\bullet}{\sigma^2}, \quad (14)$$

to calculate r_H for a SMBH of given mass,

$$r_H \approx 13.1 \left(\frac{M_\bullet}{M_8} \right)^{0.54} [\text{pc}]. \quad (15)$$

Here M_8 corresponds to $10^8 M_\odot$ and for reasons of computational feasibility we neglected the intrinsic scatter of the $M_\bullet - \sigma$ relation. This is useful when dealing with averaged quantities like the impact of stellar disruptions for the growth history of the majority of SMBHs. Some studies may instead be interested in individual systems and the extrapolation formalism can easily be replaced by direct measurements of M_\bullet, r_H and σ instead of using the values from

the $M_\bullet - \sigma$ relation. This also holds for the choice of the relevant tidal disruption radius,

$$r_{\text{cap}} = g r_\star \left(\frac{M_\bullet}{M_\star} \right)^{\frac{1}{3}}, \quad (16)$$

where g is a parameter depending on the stellar polytrope, mass and spin of the black hole as well as the trajectory of the star. Black holes below $10^7 M_\odot$ and solar like stars are well approximated by $g \approx 1$ (Kochanek 1992). A more detailed discussion of r_{cap} can be found in Appendix A.

The relevant astrophysical timescale is obtained through the computation of the crossing time $t_{\text{cr}}(r_H) = \frac{2r_H}{\sigma(r_H)}$ at the influence radius r_H of the black hole in comparison with that of our numerical integrations. The number of disruption events within the given timescale is obtained from the derived capture rate¹¹ $\dot{C}(N, r_{\text{cap}}^{\text{sim}}) = a(r_{\text{cap}}^{\text{sim}}) N^b$. Here N refers to the total number of (real) stars with the averaged mass M_\star in the bulge component or whole elliptical galaxy. It is assumed to be $N = \frac{100M_\bullet}{M_\star}$ in accordance with our numerical integrations, whereas $a(r_{\text{cap}}^{\text{sim}})$ is extrapolated to the black hole mass of interest by using the $T = 100$ values for the parameters a^{12} . The parameter b is assumed to be unrelated to the capture radius and is hence taken to be constant at $b = 0.83 \pm 0.01$. In fact Eq. 6 predicts the slope parameter b to be unrelated to the capture radius. Nevertheless a minor change in b towards smaller values of $r_{\text{cap}}^{\text{sim}}$ cannot be rejected given the b values of Table 1 at $T = 100$. This might be explained by a combination of timing issues, simplified assumptions of our analytical approach or is purely statistical in nature. Therefore the parameter b is extrapolated (by linear and power law regressions) down to the required values of $r_{\text{cap}}^{\text{sim}}$ in order to test its impact on the capture rates. The impact is found to be moderate because $r_{\text{cap}}^{\text{sim}}$ has to be extrapolated down to $r_{\text{cap}}^{\text{sim}} = (0.06 - 0.07) \cdot 10^{-7}$ (depending on the used $M_\bullet - \sigma$ -relation) for the largest black hole with $10^7 M_\odot$. While the capture rate would be unaffected for the least-massive black holes, it would drop by a factor of 2 for the most-massive ones. Increasing uncertainties of these values due to the propagation of error analysis strongly overlaps with those of fixed b . For the purposes of this study we therefore assume the parameter b to be independent of $r_{\text{cap}}^{\text{sim}}$ and refer the reader to § 7 for a more critical discussion on that topic as well as of the improvements left for future work.

Finally for an individual galactic nucleus hosting a SMBH of mass M_\bullet , with a radius of influence r_H , velocity dispersion $\sigma(r = r_H)$, capture radius r_{cap} and a stellar population with the mean mass M_\star , a very general expression for the capture rate inferred from the numerical integration

can be obtained by applying Eq. 14:

$$\dot{C}_{\text{astro}} = 0.00061 \left(\frac{M_\bullet}{M_\star} \right)^{0.951} r_H^{-1.363} r_\star^{0.363} g^{0.363} \sigma \quad (17)$$

The validity of Eq. 17 covers the parameter range of IMBHs as well as SMBHs up to $M_\bullet \approx 10^7 M_\odot$. In the following section we explicitly make use of the $M_\bullet - \sigma$ relation and assume only solar like stars as well as $g = 1$.

6.2 Disruption rates of IMBHs & SMBHs

By applying the extrapolation formalism from section §6.1, the integrations yield the following expression for the capture rate of real astrophysical galaxies:

$$\dot{C}(M_\bullet) = 6.29 \cdot 10^{-8} \left(\frac{M_\bullet}{M_\odot} \right)^{0.446} [\text{yr}^{-1}]. \quad (18)$$

For comparison the results are also extrapolated according to an older version of the $M_\bullet - \sigma$ relation from Ferrarese & Ford (2005) to illustrate the dependence of the capture rate on systematic black hole mass determinations:

$$\dot{C}(M_\bullet) = 3.54 \cdot 10^{-7} \left(\frac{M_\bullet}{M_\odot} \right)^{0.353} [\text{yr}^{-1}]. \quad (19)$$

These results holds for nonrotating isotropic galaxies or globular clusters with cuspy inner density profiles $\rho(r) \propto r^\alpha$, where the density power law index is $\alpha \approx -1.5$. Eq. 18 and 19 should not be applied to black holes with masses larger than $10^7 M_\odot$. The uncertainties correspond to about 50% of the values (see Table 2). The interested reader is referred to Appendix B for a much more detailed description of how the numerical results are extrapolated to realistic galaxies. The astrophysical disruption rates of stars (including the statistical uncertainties) for some exemplary black holes are summarized in Table 2. We also calculate the disruption rates for IMBHs in order to compare them with previous simulations (Baumgardt et al. 2004a).

The expected number of tidal disruption events in galactic nuclei containing black holes of 10^6 to $10^7 M_\odot$ inferred from the numerical integrations are in good agreement with recent optical based surveys (van Velzen et al. 2010). While their study yields the rate for tidal flares per galaxy to be $\dot{C} = 3(^{+4}_{-2}) \cdot 10^{-5} \text{yr}^{-1}$, the results obtained from the present simulations give $\dot{C} = 3.0(\pm 1.4) - 8.3(\pm 4.2) \cdot 10^{-5} \text{yr}^{-1}$ for black holes in the mass range 10^6 to $10^7 M_\odot$.

The simulations also offer some clues about the growth of IMBHs and SMBHs in the lower mass range. We observe only a modest impact of the black hole mass on the capture rate. For a mass range over four orders of magnitude, the capture rate increases only by a factor 25-60 depending on the used scaling relation. The relaxation driven growth of massive black holes by stellar disruptions is thus only important for IMBHs and SMBHs up to several $10^5 M_\odot$. IMBHs should easily double their mass within a few Gyr in perfect agreement with earlier studies (Baumgardt et al. 2004a). Much more massive black holes must have grown by different processes rather than the relaxation driven infall of stars, in good agreement with the findings of Yu & Tremaine (2002) and gas accretion and feedback

¹¹ The capture rates $\dot{C}(N)$ from the numerical computations are normalized to one N-body time unit i.e. $\frac{1}{2\sqrt{2}}$ crossing time at the virial radius $r_{\text{vir}} = 1$ and must be scaled down to one crossing time at the influence radius of the black hole in order to become synchronized with the astrophysical timescale t_{cross} .

¹² At least three different capture radii must be simulated to allow for non linear extrapolation of the parameter $a(r_{\text{cap}}^{\text{sim}})$. This is required for the extrapolation to different black hole sizes/masses.

$M_{\bullet} (10^6 M_{\odot})$	Schulze & Gebhardt (2011)		
	$\dot{C} (10^{-5} \text{ yr}^{-1})$	$T_{2D} (H_0^{-1})$	$\bar{L} (\text{ergs}^{-1})$
0.001	0.14 ± 0.06	0.11 ± 0.05	$3.9 \pm 1.7 \cdot 10^{39}$
0.01	0.38 ± 0.17	0.39 ± 0.18	$1.1 \pm 0.5 \cdot 10^{40}$
0.05	0.8 ± 0.4	0.9 ± 0.4	$2.2 \pm 1.0 \cdot 10^{40}$
0.1	1.1 ± 0.5	1.4 ± 0.7	$3.0 \pm 1.4 \cdot 10^{40}$
0.25	1.6 ± 0.8	2.3 ± 1.1	$4.5 \pm 2.2 \cdot 10^{40}$
0.5	2.2 ± 1.0	3.4 ± 1.6	$6.2 \pm 3.0 \cdot 10^{40}$
1	3.0 ± 1.4	4.9 ± 2.4	$8.4 \pm 4.1 \cdot 10^{40}$
2	4.0 ± 2.0	7.3 ± 3.6	$1.1 \pm 0.6 \cdot 10^{41}$
4	5.5 ± 2.7	11 ± 5	$1.6 \pm 0.8 \cdot 10^{41}$
10	8.3 ± 4.2	18 ± 9	$2.4 \pm 1.2 \cdot 10^{41}$

$M_{\bullet} (10^6 M_{\odot})$	Ferrarese & Ford (2005)		
	$\dot{C} (10^{-5} \text{ yr}^{-1})$	$T_{2D} (H_0^{-1})$	$\bar{L} (\text{ergs}^{-1})$
0.001	0.40 ± 0.17	0.04 ± 0.02	$1.1 \pm 0.5 \cdot 10^{40}$
0.01	0.90 ± 0.40	0.16 ± 0.07	$2.6 \pm 1.2 \cdot 10^{40}$
0.05	1.6 ± 0.7	0.46 ± 0.21	$4.5 \pm 2.1 \cdot 10^{40}$
0.1	2.0 ± 0.9	0.72 ± 0.34	$5.8 \pm 2.7 \cdot 10^{40}$
0.25	2.8 ± 1.3	1.3 ± 0.6	$8.0 \pm 3.8 \cdot 10^{40}$
0.5	3.6 ± 1.7	2.0 ± 1.0	$1.0 \pm 0.5 \cdot 10^{41}$
1	4.6 ± 2.2	3.2 ± 1.5	$1.3 \pm 0.6 \cdot 10^{41}$
2	5.8 ± 2.8	5.0 ± 2.5	$1.7 \pm 0.8 \cdot 10^{41}$
4	7.4 ± 3.7	7.9 ± 3.9	$2.1 \pm 1.0 \cdot 10^{41}$
10	10.3 ± 5.2	14 ± 7	$2.9 \pm 1.5 \cdot 10^{41}$

Table 2. The expected number of stellar disruption events \dot{C} for solar like stars by supermassive black holes up to $M_{\bullet} \leq 10^7 M_{\odot}$. For comparison our numerical results are extrapolated according to an older version of the $M_{\bullet} - \sigma$ -relation (Ferrarese & Ford 2005) and the most recent one (Schulze & Gebhardt 2011). Within a factor of two they agree with each other. T_{2D} is the time needed to double the initial mass of the black hole in units of the Hubble time H_0^{-1} . Only one half of the stellar mass is assumed to become accreted by the black hole (Rees 1988). Finally the time averaged mean luminosity $\bar{L} = 0.5\epsilon\dot{C}M_{\odot}c^2$ of these black holes is calculated by assuming the efficiency parameter of matter to energy conversion to be $\epsilon = 0.1$. The motivation behind is to compare these energies with potentially detectable left overs of relativistic outflows which may become deposited into the surrounding medium after tidal disruption events (Crocker & Aharonian 2011; Giannios & Metzger 2011; van Velzen et al. 2011). However the deposited energy strongly depends on the formation rate of relativistic jet outflows and may be significantly overestimated by us (Bower 2011). Nevertheless these deposited energies might be relevant for studies aiming to make a robust detection of dark matter annihilation signals in galactic bulges, dwarf galaxies or globular clusters hosting a central black hole. These results have relevance for galaxies with cuspy density profiles with slope parameters $\alpha \approx -1.5$ within the inner most few pc.

models (Silk & Rees 1998; Fabian 1999; Murray et al. 2005)¹³.

Our findings exclude any relevance for establishing the $M_{\bullet} - \sigma$ relation from stellar disruptions in density profiles similar to those of the simulations. This is due to the relatively small capture rate and hence large doubling times ($T_{2D} > H_0^{-1}$) for black holes more massive than

$10^6 M_{\odot}$. If for example the initial mass of a SMBH is strongly under-massive with respect to the $M_{\bullet} - \sigma$ relation, the feeding from tidal disruptions events alone might not be sufficient enough to bring it close to the observed relation for galaxies at $z \approx 0$. On the other hand if stellar disruptions dominate the growth of the least-massive black holes there is no obvious reason why these black holes should follow the $M_{\bullet} - \sigma$ relation. By now assuming the $M_{\bullet} - \sigma$ relation to be established for a primordial gas rich globular cluster (or galactic nucleus), which nowadays remains in isolation and without gas to drive new star formation, the resulting IMBH (or SMBH, at least if it is not too massive) should nowadays be more massive than expected from the $M_{\bullet} - \sigma$ relation due to subsequent tidal disruption events. It is very tempting to connect these results to the case of ω -Centauri (Noyola et al. 2010). Tidal disruption events might therefore have implications for the search and existence of IMBHs in globular clusters. Of course in order to proof its relevance for IMBHs, the use of the $M_{\bullet} - \sigma$ relation in the extrapolation formalism from numerical simulations to galactic nuclei (Appendix B) must be replaced by more direct observational data because the extrapolated values strongly depend on the validity of this scaling relation. Tidal disruption events complicate the understanding of the relevant processes which drive the evolution of galaxies and their central black holes. Especially as the impact of disruption events for the mass growth of black holes strongly depends on their initial mass.

In spite of this it might be interesting to relate these findings to a recent study Kormendy et al. (2011) in which observational evidence for secular growth processes of black holes in disks and pseudobulges is found. The capture rate for rotation-supported models like rotating bulges or pseudo bulges should be enhanced compared to nonrotating models. These objects are expected to form from rotating bar instabilities (Kormendy & Kennicutt 2004) and the relative velocities between two or more particles are generally lower. Therefore two-body relaxation processes would be even stronger.

However the overall picture of black hole growth across cosmic times by tidal disruptions might be complicated even more due to the dynamical evolution of the density profile and a variable fraction of the initial stellar mass which finally becomes accreted by the black hole. Our conclusions regarding the growth history of IMBHs and SMBHs events should only hold for density profiles resembling those of our simulations and by assuming that a fraction of one half (or more) of the initial stellar mass becomes accreted by the black hole (Rees 1988). In fact some effects can considerably reduce this fraction and complicate the efforts to estimate the significance of tidal disruption events for the overall growth history of black holes. Recent hydrodynamical simulations suggest that for loss cone stars on nearly parabolic orbits, most of the stellar matter is ejected within the first orbit and then later on due to powerful shocks which may be energetic enough to ignite thermonuclear reactions unbinding large amounts of stellar mass (Brassart & Luminet 2008; Guillochon et al. 2009). Secondly and especially relevant for black holes in the lower mass range, accretion luminosities far in excess of

¹³ The growth of the very early population of SMBHs may also be dominated by stellar disruptions in isothermal cusps (Zhao et al. 2002). See the information in the text below.

the Eddington limit (Strubbe & Quataert 2011) may blow away most of the remaining gas. In the end the growth of these black holes due to tidal disruption events may be insignificant even for very large capture rates of several events per 10^6 yr.

7 CRITICAL DISCUSSION AND OUTLOOK FOR FUTURE WORK

To the best of our knowledge this study reports for the first time the expected tidal disruption rate of stars by SMBHs up to $10^7 M_\odot$ obtained by direct N-body integrations. N-body computations offer a large amount of advantages over analytical studies. They can handle several physical effects simultaneously while most analytical studies are forced to simplify at least some of the dynamics. On the other hand direct N-body integrations aiming to infer astrophysically relevant numbers of stellar disruption events are confronted by their own limitations and difficulties. In this section we will critically review limitations of our own simulations as well as improvements and ideas left for future work.

(a) In Table 2 we calculate among other values the required timescale T_{2D} for doubling the mass of a black hole of given initial mass. This timescale is computed from the total number of captures averaged over 100 N-body time units (see Table 1). We recommend the reader to regard the doubling time T_{2D} only as some reference guide. When expressed in physical time, our simulations last only a fraction of one H_0^{-1} (between several 10^7 and one 10^9 years) and may not represent much longer time episodes. Moreover we assumed one half of the disrupted star to be accreted by the black hole. There exist two effects that can reduce the amount of stellar matter which finally becomes swallowed by the black hole. First, if the tidal stripping occurs from a nearly parabolic orbit, hydrodynamical simulations suggest one half of its mass to be lost within its first path (Guillochon et al. 2009) and large quantities of the remaining mass to be blown away by shocks and thermonuclear reactions later on (Brassart & Luminet 2008). Second, very small black holes might temporarily generate luminosities far in excess of the Eddington limit (Strubbe & Quataert 2011) and most of the remaining matter may finally be blown away instead of being swallowed by the black hole. This would invalidate our conclusions regarding the growth history of small black holes where we assumed one half of the stellar mass to be accreted. Nevertheless the inferred capture rate should be valid for all galaxies or stellar clusters with density profiles comparable to our simulated ones.

(b) With current generations of GPUs it is unthinkable to simulate galaxy models with realistic numbers of stars with direct N-body integration methods. The only way to obtain stellar disruption rates for SMBHs in the centers of galaxies is to simulate as many models as possible to infer all relevant N-dependent systematics affecting this rate. Afterwards the results can be extrapolated. However it is important not to do this for only one given black hole capture radius but for many black hole configurations. Therefore all these simulations must be repeated for several capture radii $r_{\text{cap}}^{\text{sim}}$ in order to extrapolate them according to the formalism in § 6.1 to the black hole of interest.

We calculate the capture rate for black hole masses in the range $10^{3-7} M_\odot$. Due to the highly nonlinear Eq. 13 we had to extrapolate parameter $r_{\text{cap}}^{\text{sim}}$ from Table 1 down to $r_{\text{cap}}^{\text{sim}} \approx 0.07 \cdot 10^{-7}$. The usage of three different black hole capture radii is thus the minimal requirement to obtain useful values under the assumption that the parameter $a(r_{\text{cap}}^{\text{sim}})$ from Eq. 11 follows a power law distribution¹⁴ with positive parameters and no offset.

There is no question that future studies must redo these simulations for different capture radii to constrain $a(r_{\text{cap}}^{\text{sim}})$ even more precisely. However this is a very time consuming task. The complete set of our Sersic $n = 4$ simulations took more than seven months to compute on five modern GPUs. Despite the large amount of needed computing power, direct integration methods like NBODY6 may exceed their limitations when the capture radius falls significantly below 10^{-7} in N-body units, especially if the mass of the black hole particle is of the order of one percent or more of the total mass¹⁵. In addition to that the statistics may worsen (due to a limited number of capture events) and must be balanced by even more simulations.

In our computations no severe $r_{\text{cap}}^{\text{sim}}$ dependence of the parameter b is evident, in accordance with theoretical considerations (Eq. 6 & 8)¹⁶. Therefore we assumed it to be constant. However we cannot exclude per se any deviation at very small capture radii. A systematic decrease in the parameter b for even smaller values of $r_{\text{cap}}^{\text{sim}}$ would only reduce the tidal disruption events of the more massive SMBHs in our sample. We plan to tackle this problem as well as to constrain the parameters $a(r_{\text{cap}}^{\text{sim}})$ and b even more precisely in the future.

(c) In this study effects from General Relativity are neglected. The relevant tidal disruption radius of a SMBH for solar like stars is several times larger than its Schwarzschild radius and relativistic effects should become strongly suppressed for radii $r \gg r_s$. This makes our assumption of neglecting GR credible. Nevertheless a fully relativistic treatment of a black hole potential yields a deeper gravitational potential than a purely Newtonian one, thus being more attractive for compact bodies like stars to be captured by the SMBH. On the other hand particle scattering by a relativistic potential may result in stronger deflection, perhaps powerful enough to reject some stars from the immediate vicinity of the black hole thereby decreasing the capture rate. The next generation of N-body integrators is expected to be sophisticated enough to address these aspects (Aarseth 2007).

Rotating black hole spacetimes should be considered, too. The cross section of a realistic black hole strongly depends on its mass and spin parameter $j = \frac{J_\bullet}{M_\bullet^2}$, where J_\bullet is the angular momentum of the black hole. The likelihood for a particle to become swallowed by the black hole depends on

¹⁴ $a(r_{\text{cap}}^{\text{sim}})$ is specified in Eq. B3.

¹⁵ Private communication with Sverre Aarseth.

¹⁶ According to the theory of angular momentum diffusion, parameter b only depend on the slope parameter of the density profile.

the spin parameter, its trajectory and angular momentum. Particles are more likely captured if they counter rotate the black hole because in this direction the effective capture radius is enlarged. It is not unreasonable to conclude that a rotating black hole embedded inside a nonrotating spherical distribution of stars will lose some of its angular momentum. On the one hand j decreases when M_\bullet becomes larger, on the other hand counter rotating particles are more likely captured. This would lower J_\bullet and thus the spin parameter j . If tidal disruption events really contribute a significant amount of mass to a specific population of black holes, it should also affect their spin values in a way which might deviate from the predictions of gas accretion models.

(d) A crucial quantity for extrapolating our numerical results to astrophysical systems is the black hole radius of influence r_H . For its evaluation we use the kinematic determination (Appendix B). We observe this radius to be roughly five to six times smaller than the dynamical radius r_g . This is the radius at which the mass in stars/particles equals the mass of the black hole. If interested readers plan to rescale our models by replacing the $M_\bullet - \sigma$ relation by directly measured data of r_H for some galaxies, it is very important that they also use the same influence radii as the ones used in our simulations and not the dynamical radii.

(e) The capture rate from our numerical results should not be applied to SMBHs above $10^7 M_\odot$. The refill of the loss cone takes a timespan of the order $T_{\text{refill}} \approx \theta_{\text{lc}}^2 T_{\text{rel}}$. The refill of the loss cone is much faster in N-body integrations than in nature, since the potentials are more cuspy and relaxation times are shorter than in reality. Therefore our simulations have only relevance for galactic nuclei where the loss cone refilling times are much shorter than H_0^{-1} . In Appendix C we show that $T_{\text{refill}} \ll H_0^{-1}$ for a black hole with a mass of $10^7 M_\odot$. This becomes also evident from Eq. 6 & 8. For black holes significantly more massive than $10^7 M_\odot$, i.e. with very large particle numbers and very smooth potentials, the critical radius becomes much larger than the influence radius of the black hole and Eq. 6 has to be replaced by Eq. 8. The latter one predicts a different behavior for $\dot{C}(N)$ such that the numerically found capture rate should not be extrapolated to black holes in excess of $10^7 M_\odot$. By inserting the relevant values from our computational findings to the systems of interest, Eq. 6 predicts the critical radius not to exceed the influence radius for black holes less massive than $10^7 M_\odot$, thus showing our simulations to be governed by processes $r_{\text{crit}} < r_H$.

(f) One could even criticize the black hole mass $M_\bullet(t=0) = 0.01$ used for our numerical computations to be too high as the black hole mass fraction in realistic galaxies is a factor of a few smaller (Magorrian et al. 1998). Nevertheless most of the relevant dynamics happens at distances of the order of the influence radius r_H whereas we use the radius of influence for the extrapolation to realistic galaxies. The choice of $M_\bullet(t=0) = 0.01$ is therefore not expected to change the capture rate significantly. In this context the usage of different capture radii instead of different initial masses $M_\bullet(t=0)$ for the extrapolation to the wide set of astrophysical SMBHs should be justified, too. The strict relation between mass and capture radius of a black hole (Eq. A1) enables variation of the latter one while keeping the former one constant in the scale-free N-body simulations. The great advantage of this strategy is given

in equal black hole influence radii, crossing times, cusp formation timescales etc. simplifying the extrapolation formalism considerably. The same holds true for the overall Sérsic $n = 4$ profiles. Not every outer bulge component or elliptical galaxy profile resembles that of a Sérsic $n = 4$ i.e. de Vaucouleurs profile. Mostly relevant for the direct number of capture events is the density profile close to r_H . For relaxation times smaller than one H_0^{-1} the formation of a cusp (up to $\alpha = -1.75$) is expected. Such a gradual change of the density profile is also found in the numerical simulations. Hence our simulations cover a large space of isotropic, non-rotating density profiles for black hole masses up to $10^7 M_\odot$.

(g) We only treat single-mass systems while galactic cores are known to be multiple-mass systems featuring additional processes like mass segregation, star formation, binary evolution, torques from anisotropic matter distributions, resonances etc. Stellar remnants like neutron stars would not be disrupted outside the event horizon and could probe much deeper potentials than solar like stars, thus complicating the gravitational dynamics and making relativistic correction terms inescapable. They would also disappear without any visible counterpart when finally captured.

(h) Finally our numerical simulations should only be regarded as a first (very) limited approach to a systematical scan of capture rates in galaxies. It would be important to extend these studies by simulating the same models for even smaller capture radii r_{ext} and longer timescales in order to reduce the need of extrapolation. It would be important to take into account rotating and triaxial stellar density profiles around the SMBH and to decrease the still rather large uncertainties. Direct N-body simulations of isothermal $\rho(r) = \frac{\sigma^2}{2\pi G r^2}$ spheres, which might represent the initial phases of elliptical galaxies and bulges best, should be performed as well. Zhao et al. (2002) found evidence for strong black hole growth in isothermal cusps. By assuming $r_{\text{cap}} \propto r_s = \frac{2GM_\bullet}{c^2}$, rewriting Eq. 5 to $\dot{C}(r) \propto \rho(r)r^2\sigma\theta_{\text{lc}}^2$ by using $r_H = \frac{GM_\bullet}{\sigma^2}$ and $\theta_{\text{lc}}^2 = \frac{2r_{\text{cap}}r_H}{r^2}$ for very massive SMBHs, one obtains $\dot{C}(r) \propto \frac{\sigma^5}{Gc^2} \cdot \left(\frac{r_H}{r}\right)^2$. Under the assumption that the capture rate is dominated by stars from r_H , the r dependence cancels out and the final mass of the black hole is $M_\bullet(t_f) = \int_{t=0}^{t=t_f} \dot{C}(r = r_H) dt \approx 10^8 M_\odot \cdot \left(\frac{\sigma}{200 \text{ km s}^{-1}}\right)^5 \left(\frac{t_f}{H_0^{-1}}\right)$. This relation is indeed in very close agreement to the observed $M_\bullet - \sigma$ relation (Zhao et al. 2002). Therefore stellar captures might contribute significantly to the growth of SMBHs in the past, especially if the loss cone refill is enhanced by mergers and/or triaxial stellar distributions.

Despite some of the details stated above, the here reported simulations represent (the first) systematic estimate for the capture rate by SMBHs of stars in galaxies with cuspy inner density profiles. This work should be followed up by simulating different capture radii $r_{\text{cap}}^{\text{sim}}$ as well as density profiles, taking relativistic correction terms into account, and by trying to find ways to infer the numbers of disruption/capture events for SMBHs with mass $> 10^7 M_\odot$.

8 CONCLUSION

We performed direct N-body simulations to obtain the number of disruption events of stars by SMBHs which are presumed to exist in the centers of most galaxies. A modified NBODY6 code was used. All computations were processed by several GPUs over several months integration time. The initial density profiles of the models were chosen to follow nonrotating isotropic Sérsic $n = 4$ profiles. We calculated numerous models with different particle numbers but otherwise equal physical parameters in order to ensure good statistics. This is required because all systematic effects depending on the total number of particles must be specified in order to extrapolate the simulations to realistic galaxies by using the formalism presented in § 6.1. The rates at which stars are captured are found to be nearly independent of the mass of the black hole. Thus only the growth over cosmic times of IMBHs and of the least massive SMBHs may be dominated by stellar disruptions. The expected tidal disruption rate is a few events every 10^5 years per galaxy for black holes in the mass range up to $10^7 M_\odot$. The feeding by stars from density profiles similar to the ones computed here bears no implications for establishing scaling relations between very massive black holes and their host galaxies. This is in agreement with conventional gas accretion/feedback models. On the other hand the growth history of the least massive black holes might be governed by more than one feeding mode (gas and star accretion). This might have implications for the search and existence of potential IMBHs in globular clusters and minor galaxies. Assuming these scaling relations (e.g. the $M_\bullet - \sigma$ relation) to be established shortly after their primordial gas rich phase billions of years ago, the nuclear black holes would continue their growth by the subsequent disruption of stars. Depending on the initial conditions, the black hole masses could nowadays lie well above the predicted values of the $M_\bullet - \sigma$ relation as long as the globular cluster remains in isolation¹⁷. On the other hand the continuous monitoring and search for tidal disruption events in globular clusters (e.g. in the Virgo Cluster) should constrain the fraction of those clusters hosting a central IMBH. By assuming 25000 globular clusters with a central black hole in the mass range $M_\bullet = 10^3 - 10^4 M_\odot$ in the Virgo Cluster of galaxies, there should be one disruption event every 10 – 25 years. Finally the performed computations indicate that the growth history of IMBHs and low mass SMBHs is diverse and not only governed by one process, i.e gas accretion. However it needs to be pointed out that there exist effects which might reduce the fraction of stellar matter which finally becomes accreted by the black hole. We assumed one half of a captured star's mass to be swallowed (Rees 1988), whereas a smaller fraction would result in even slower growth rates. Thus our conclusions regarding the growth history may change if small black holes gather only tiny fractions of the total initial stellar mass. Future studies can use the reported capture rate $\dot{C}(M_\bullet)$ to deduce more realistic growth rates $\dot{M}(M_\bullet)$ by taking more appropriate values for the fraction of accreted matter into account. It would also be interesting to extend these studies

to the most-massive black holes as well as constraining the capture rate for different profiles.

ACKNOWLEDGMENTS

We warmly thank Ole Marggraf and Fabian Lüghausen for their readiness to assist us in some technical problems as well as Sverre Aarseth, Jan Pflamm-Altenburg and Sambaran Banerjee for inspiring discussions about black holes and numerical integrators. Special thanks are devoted for Ingo Thies and Matthias Kruckow. The work of this paper was supported by the German Research Foundation (DFG) through grants BA 2886/4-2 within the priority programme 1177 “Witnesses of Cosmic History: Formation and Evolution of Black Holes, Galaxies and Their Environment”. H.B. acknowledges support from the Australian Research Council through Future Fellowship grant FT0991052.

REFERENCES

- Aarseth S. J., 1999, *PASP*, 111, 1333
- Aarseth S. J., 2003, *Gravitational N-Body Simulations*
- Aarseth S. J., 2007, *MNRAS*, 378, 285
- Alexander T., Hopman C., 2009, *ApJ*, 697, 1861
- Amaro-Seoane P., Freitag M., Spurzem R., 2004, *MNRAS*, 352, 655
- Bahcall J. N., Wolf R. A., 1976, *ApJ*, 209, 214
- Bailey V. C., Davies M. B., 1999, *MNRAS*, 308, 257
- Baumgardt H., Gualandris A., Portegies Zwart S., 2006, *MNRAS*, 372, 174
- Baumgardt H., Hopman C., Portegies Zwart S., Makino J., 2006, *MNRAS*, 372, 467
- Baumgardt H., Makino J., Ebisuzaki T., 2004a, *ApJ*, 613, 1133
- Baumgardt H., Makino J., Ebisuzaki T., 2004b, *ApJ*, 613, 1143
- Berczik P., Merritt D., Spurzem R., Bischof H., 2006, *ApJ*, 642, L21
- Binney J., Tremaine S., 2008, *Galactic Dynamics: Second Edition*. Princeton University Press
- Bower G. C., 2011, *ApJ*, 732, L12+
- Brassart M., Luminet J.-P., 2008, *A&A*, 481, 259
- Burkert A., Tremaine S., 2010, *ApJ*, 720, 516
- Caon N., Capaccioli M., D’Onofrio M., 1993, *MNRAS*, 265, 1013
- Cappelluti N., Ajello M., Rebusco P., Komossa S., Bongiorno A., Clemens C., Salvato M., Esquej P., Aldcroft T., Greiner J., Quintana H., 2009, *A&A*, 495, L9
- Casertano S., Hut P., 1985, *ApJ*, 298, 80
- Chandrasekhar S., 1943a, *ApJ*, 97, 255
- Chandrasekhar S., 1943b, *ApJ*, 97, 263
- Chandrasekhar S., 1943c, *ApJ*, 98, 54
- Chatterjee P., Hernquist L., Loeb A., 2002, *ApJ*, 572, 371
- Ciotti L., Bertin G., 1999, *A&A*, 352, 447
- Crocker R. M., Aharonian F., 2011, *Physical Review Letters*, 106, 101102
- Dale J. E., Davies M. B., Church R. P., Freitag M., 2009, *MNRAS*, 393, 1016
- Duncan M. J., Shapiro S. L., 1983, *ApJ*, 268, 565

¹⁷ The relevant velocity dispersion σ should therefore not increase.

- Esquej P., Saxton R. D., Komossa S., Read A. M., Freyberg M. J., Hasinger G., García-Hernández D. A., Lu H., Rodríguez Zaurín J., Sánchez-Portal M., Zhou H., 2008, *A&A*, 489, 543
- Fabian A. C., 1999, *MNRAS*, 308, L39
- Ferrarese L., Ford H., 2005, *Space Science Reviews*, 116, 523
- Ferrarese L., Merritt D., 2000, *ApJ*, 539, L9
- Frank J., Rees M. J., 1976, *MNRAS*, 176, 633
- Freitag M., Amaro-Seoane P., Kalogera V., 2006, *ApJ*, 649, 91
- Freitag M., Dale J. E., Church R. P., Davies M. B., 2008, in M. Bureau, E. Athanassoula, & B. Barbuy ed., *IAU Symposium Vol. 245 of IAU Symposium, Dynamics of galactic nuclei: mass segregation and collisions*. pp 211–214
- Fukushige T., Makino J., Kawai A., 2005, *PASJ*, 57, 1009
- Gebhardt K., Adams J., Richstone D., Lauer T. R., Faber S. M., Gültekin K., Murphy J., Tremaine S., 2011, *ArXiv e-prints*
- Gebhardt K., Bender R., Bower G., Dressler A., Faber S. M., Filippenko A. V., Green R., Grillmair C., Ho L. C., Kormendy J., Lauer T. R., Magorrian J., Pinkney J., Richstone D., Tremaine S., 2000, *ApJ*, 539, L13
- Gebhardt K., Thomas J., 2009, *ApJ*, 700, 1690
- Gezari S., Basa S., Martin D. C., Bazin G., Forster K., Milliard B., Halpern J. P., Friedman P. G., Morrissey P., Neff S. G., Schiminovich D., Seibert M., Small T., Wyder T. K., 2008, *ApJ*, 676, 944
- Gezari S., Heckman T., Cenko S. B., Eracleous M., Forster K., Gonçalves T. S., Martin D. C., Morrissey P., Neff S. G., Seibert M., Schiminovich D., Wyder T. K., 2009, *ApJ*, 698, 1367
- Giannios D., Metzger B. D., 2011, *ArXiv e-prints*
- Gualandris A., Merritt D., 2007, *ArXiv e-prints*
- Guillochon J., Ramirez-Ruiz E., Rosswog S., Kasen D., 2009, *ApJ*, 705, 844
- Gültekin K., Richstone D. O., Gebhardt K., Lauer T. R., Tremaine S., Aller M. C., Bender R., Dressler A., Faber S. M., Filippenko A. V., Green R., Ho L. C., Kormendy J., Magorrian J., Pinkney J., Siopis C., 2009, *ApJ*, 698, 198
- Halpern J. P., Gezari S., Komossa S., 2004, *ApJ*, 604, 572
- Häring N., Rix H., 2004, *ApJ*, 604, L89
- Heggie D. C., Mathieu R. D., 1986, in P. Hut & S. L. W. McMillan ed., *The Use of Supercomputers in Stellar Dynamics Vol. 267 of Lecture Notes in Physics*, Berlin Springer Verlag, Standardised Units and Time Scales. pp 233–+
- Hilker M., Baumgardt H., Infante L., Drinkwater M., Evstigneeva E., Gregg M., 2007, *A&A*, 463, 119
- Hopkins P. F., Hernquist L., 2010, *MNRAS*, 407, 447
- Hopkins P. F., Quataert E., 2010, *MNRAS*, 407, 1529
- Hopman C., 2009, *ApJ*, 700, 1933
- Ivanov P. B., Chernyakova M. A., 2006, *A&A*, 448, 843
- Kochanek C. S., 1992, *ApJ*, 385, 604
- Komatsu E., Dunkley J., Nolte M. R., Bennett C. L., Gold B., Hinshaw G., Jarosik N., Larson D., Limon M., Page L., Spergel D. N., Halpern M., Hill R. S., Kogut A., Meyer S. S., Tucker G. S., Weiland J. L., Wollack E., Wright E. L., 2009, *ApJ*, 180, 330
- Komossa S., 2002, in M. Gilfanov, R. Sunyaev, & E. Churazov ed., *Lighthouses of the Universe: The Most Luminous Celestial Objects and Their Use for Cosmology X-Ray Evidence for SMBHs in Non-Active Galaxies: Detection of X-Ray Flare Events, Interpreted as Tidal Disruptions of Stars by SMBHs*. pp 436–+
- Komossa S., Halpern J., Schartel N., Hasinger G., Santos-Lleo M., Predehl P., 2004, *ApJ*, 603, L17
- Komossa S., Zhou H., Rau A., Dopita M., Gal-Yam A., Greiner J., Zuther J., Salvato M., Xu D., Lu H., Saxton R., Ajello M., 2009, *ApJ*, 701, 105
- Kormendy J., Bender R., 1996, *ApJ*, 464, L119+
- Kormendy J., Bender R., 2009, *ApJ*, 691, L142
- Kormendy J., Bender R., Cornell M. E., 2011, *Nat*, 469, 374
- Kormendy J., Kennicutt Jr. R. C., 2004, *A&AR*, 42, 603
- Kormendy J., Richstone D., 1995, *A&AR*, 33, 581
- Kroupa P., 2001, *MNRAS*, 322, 231
- Lai D., Rasio F. A., Shapiro S. L., 1994, *ApJ*, 437, 742
- Lauer T. R., Faber S. M., Richstone D., Gebhardt K., Tremaine S., Postman M., Dressler A., Aller M. C., Filippenko A. V., Green R., Ho L. C., Kormendy J., Magorrian J., Pinkney J., 2007, *ApJ*, 662, 808
- Lightman A. P., Shapiro S. L., 1977, *ApJ*, 211, 244
- Löckmann U., Baumgardt H., Kroupa P., 2010, *MNRAS*, 402, 519
- Magorrian J., Tremaine S., 1999, *MNRAS*, 309, 447
- Magorrian J., Tremaine S., Richstone D., Bender R., Bower G., Dressler A., Faber S. M., Gebhardt K., Green R., Grillmair C., Kormendy J., Lauer T., 1998, *AJ*, 115, 2285
- Merritt D., 2005, in A. Merloni, S. Nayakshin, & R. A. Sunyaev ed., *Growing Black Holes: Accretion in a Cosmological Context Interaction of Supermassive Black Holes with Their Stellar and Dark Matter Environments*. pp 221–235
- Merritt D., Poon M. Y., 2004, *ApJ*, 606, 788
- Merritt D., Vasiliev E., 2010, *ArXiv e-prints*
- Merritt D., Wang J., 2005, *ApJ*, 621, L101
- Milosavljević M., Merritt D., Ho L. C., 2006, *ApJ*, 652, 120
- Morris M., 1993, *ApJ*, 408, 496
- Murray N., Quataert E., Thompson T. A., 2005, *ApJ*, 618, 569
- Norman C., Silk J., 1983, *ApJ*, 266, 502
- Novikov I. D., Frolov V. P., 1989, *Physics of black holes*
- Noyola E., Gebhardt K., Kissler-Patig M., Lützgendorf N., Jalali B., de Zeeuw P. T., Baumgardt H., 2010, *ApJ*, 719, L60
- Perets H. B., Hopman C., Alexander T., 2007, *ApJ*, 656, 709
- Poon M. Y., Merritt D., 2001, *ApJ*, 549, 192
- Poon M. Y., Merritt D., 2002, *ApJ*, 568, L89
- Press W. H., Teukolsky S. A., Vetterling W. T., Flannery B. P., 1992, *Numerical Recipes in Fortran 77*, second edn. Cambridge University Press, Cambridge
- Preto M., Amaro-Seoane P., 2010, *ApJ*, 708, L42
- Rees M. J., 1988, *Nat*, 333, 523
- Schawinski et al. K., 2006, *Nat*, 442, 888
- Schulze A., Gebhardt K., 2011, *ApJ*, 729, 21
- Sersic J. L., 1968, *Atlas de galaxies australes*
- Silk J., Rees M. J., 1998, *A&A*, 331, L1
- Soltan A., 1982, *MNRAS*, 200, 115
- Spitzer L., 1987, *Dynamical evolution of globular clusters*
- Spitzer Jr. L., Harm R., 1958, *ApJ*, 127, 544
- Stone N., Loeb A., 2010, *ArXiv e-prints*
- Strubbe L. E., Quataert E., 2011, *MNRAS*, pp 696–+

- Trujillo I., Erwin P., Asensio Ramos A., Graham A. W., 2004, *AJ*, 127, 1917
 Ulmer A., 1999, *ApJ*, 514, 180
 van Velzen S., Farrar G. R., Gezari S., Morrell N., Zaritsky D., Ostman L., Smith M., Gelfand J., 2010, *ArXiv e-prints*
 van Velzen S., Koerding E., Falcke H., 2011, *ArXiv e-prints*
 Wang J., Merritt D., 2004, *ApJ*, 600, 149
 Yu Q., Tremaine S., 2002, *MNRAS*, 335, 965
 Zhao H., Haehnelt M. G., Rees M. J., 2002, *New Astron.*, 7, 385

APPENDIX A: THE TIDAL DISRUPTION/CAPTURE RADIUS

The disruption radius at which a star is torn apart by tidal forces such that roughly one half of its matter will become accreted by the black hole, is a function of the mass and spin of the black hole as well as the trajectory, internal structure, size and mass of the star. A star is disrupted outside the event horizon if the black hole mass is smaller than a certain limit (Lai et al. 1994; Binney & Tremaine 2008). For typical solar-type stars with masses $M_\star \approx 1M_\odot$ and radii $r_\star \approx 1R_\odot$ the mass of the black hole must be smaller than $M_\bullet \leq 10^8 M_\odot$ to disrupt the star before reaching the event horizon. A strongly spinning black hole dramatically alters the situation (Ivanov & Chernyakova 2006). Sufficiently massive black holes swallow stars as a whole. The General Theory of Relativity predicts the radius where a star is doomed to enter a very massive black hole to be larger than the actual Schwarzschild-radius r_s (Novikov & Frolov 1989). Stars on initial Keplerian orbits coming from infinity with pericentre distances $q \leq 4r_s$ will be swallowed by the black hole as long as $(\frac{v_\infty}{c})^2 \ll 1$. The particles in the N-body simulations do not come from infinity but their speed at the apocentre distance is much lower than the corresponding speed of light and the capture radius of $r_{\text{cap}} = 4r_s$ seems to be the most natural and best approximation for the behaviour of a realistic (extremely massive $\geq 10^8 M_\odot$) black hole. This approximation also holds for the bound particles around the black hole which are most likely swallowed. The ratio $(\frac{v_{\text{apo}}}{v_{\text{peri}}})^2$ for apocentre distances of $10^{-4} - 10^{-2}$ is always much smaller than one. For our purposes the capture radius can finally be defined as:

$$r_{\text{cap}} = \begin{cases} gr_\star \left(\frac{M_\bullet}{M_\star}\right)^{\frac{1}{3}} & : M_\bullet \lesssim 10^8 M_\odot \\ \frac{8GM_\bullet}{c^2} & : M_\bullet \gtrsim 10^8 M_\odot \end{cases} \quad (\text{A1})$$

The parameter g , which is of the order of one, depends on many parameters and can be taken from Kochanek (1992); Lai et al. (1994); Ivanov & Chernyakova (2006).

APPENDIX B: EXTRAPOLATION

In the following part we give a more detailed description of the formalism by which the here obtained capture rates (Table 1) can be scaled up to realistic bulges of galaxies or elliptical galaxies.

(a) From the relation

$$\frac{r_{\text{cap}}}{r_H} \Big|_{\text{sim}} = \frac{r_{\text{cap}}}{r_H} \Big|_{\text{astro}} \quad (\text{B1})$$

the required capture radius $r_{\text{cap}}^{\text{sim}}$ for a black hole of mass M_\bullet must be obtained by using astronomical observations of individual galaxies or by making use of the $M_\bullet - \sigma$ relation from Schulze & Gebhardt (2011). If in the near future much larger samples of measured SMBH masses allow for more accurate values, it will be no problem to implement them into this formalism. By combining Eq. B1 with the disruption radius $r_{\text{cap}} = gr_\star \left(\frac{M_\bullet}{M_\star}\right)^{\frac{1}{3}}$ and the expression for the radius of influence $r_H \approx 13.1 \left(\frac{M_\bullet}{M_8}\right)^{0.54}$ [pc] which is derived from the $M_\bullet - \sigma$ scaling relation, $r_{\text{cap}}^{\text{sim}}$ follows:

$$r_{\text{cap}}^{\text{sim}} \approx 4g \cdot 10^{-9} \left(\frac{M_\bullet}{M_8}\right)^{-0.2067} \quad (\text{B2})$$

It specifies the required capture radius in the scale-free N-body integrations for the astrophysical black hole of interest. Afterwards the function $a(r_{\text{cap}}^{\text{sim}})$ must be evaluated from the values in Table 1:

$$a(r_{\text{cap}}^{\text{sim}}) = 0.023(\pm 0.006) \left(r_{\text{cap}}^{\text{sim}}\right)^{0.363(\pm 0.020)} \quad (\text{B3})$$

yields a reasonable approximation¹⁸ for the extrapolation of the parameter a from Eq. 11 to any desired $r_{\text{cap}}^{\text{sim}}$. For the purposes of this paper the slope parameter $b = 0.83$ is assumed to be independent of $r_{\text{cap}}^{\text{sim}}$. As already mentioned in § 6.1 the parameter g accounts for the stellar model and mass of the black hole. It is of the order of one (Kochanek 1992; Lai et al. 1994; Ivanov & Chernyakova 2006). For simplicity we use $g = 1$ which is a reasonable assumption for nonrotating black holes less massive than $M_\bullet = 10^7 M_\odot$ and solar mass stars. Eq. B2 assumes all stars to be disrupted before entering the horizon.

(b) The dynamical timescale t_{sim} of the N-body particles inside the sphere of influence r_H has to be calculated according to $t_{\text{sim}} = \frac{2r_H}{\sigma(r=r_H)} \approx 0.008$. It is used as a reference for timing issues when compared to the relevant astrophysical timescales t . To ease the extrapolation of the numerical results to astrophysical systems, we compute the time averaged influence radius r_H . Representative for all models we calculate r_H and t_{sim} from the 25 k, 50 k, 75 k, 150 k and 250 k models. For the calculation of the radius of influence we bin the particles in cylindrical shells of thickness $\Delta r = 0.001$ and measure for each configuration the one dimensional velocity dispersion (line of sight velocity) $\sigma_i^2 = \frac{\sum_i v_{i,z}^2}{N_i}$ in order to obtain $\sigma(r)_{\text{sim}}^2$. Here N_i is the number of particles within each configuration. We choose the line of sight axis to be parallel to the z-axis. Afterwards $\sigma_{\text{bh},i}^2 = \frac{M_\bullet(t)}{3N_i} \cdot \left(\sum_{i=1}^{N_i} \frac{1}{r_i}\right)$ is calculated for each cylindrical shell to obtain $\sigma(r)_{\text{bh}}^2$, here $r_i = \sqrt{x_i^2 + y_i^2 + z_i^2}$. The factor 3 in the denominator is used for the normalization to the relevant line of sight velocity inside the isotropic distribution. The radius of influence r_H is then calculated to be the radius at which $\frac{\sigma(r)_{\text{sim}}^2}{\sigma(r)_{\text{bh}}^2} = 2$. We note that in N-body units $G = 1$. The position of the black hole is used as the reference center and the mass gain of the black hole is taken into account. For the time averaged influence radius and velocity

¹⁸ $Q = 0.89$ without rescaling $\chi_\mu = 1$. Afterwards the uncertainties are taken directly from the covariance matrix. Renormalization induces the errors to be uncorrelated to each other.

dispersion we obtain $r_h \approx 0.005$ and $\sigma(r = r_H) \approx 1.26$. The black hole influence radius is 5 – 6 times smaller than the dynamical radius.

(c) Subsequently the astrophysical dynamical timescale $t_{\text{cr}}(r_H) = \frac{2r_H}{\sigma} \Big|_{\text{astro}}$ of the matter distribution within the influence radius of the astrophysical galaxy must be computed for the black hole of given mass by using $r_H \approx 13.1 \left(\frac{M_\bullet}{M_8}\right)^{0.54} [\text{pc}]$ and $\sigma \approx 200 \left(\frac{M_8}{1.5135}\right)^{0.23} [\text{kms}^{-1}]$ from Schulze & Gebhardt (2011).

(d) The number of stars N in the astrophysical galaxy must be specified. For simplicity we assume all stars to have the same mass $\langle M_\star \rangle = 1M_\odot$. A coarse estimate for the number of stars can be computed by:

$$N = \frac{100M_\bullet}{\langle M_\star \rangle}. \quad (\text{B4})$$

The choice of $\langle M_\star \rangle = 1M_\odot$ depends on the stellar mass function and seems to be a reasonable assumption for galactic nuclei where mass segregation is important (Freitag et al. 2006; Kroupa 2001; L\"ockmann et al. 2010). The factor 100 accounts for the fraction of bulge mass to black hole mass in accordance with our simulations.

(e) Finally the disruption rate of stars by massive black holes can be evaluated. In a first step the numerically inferred number of captures $\dot{C}(N)$ per N-body time unit (Table 1) must be normalized to the relevant crossing time $t_{\text{sim}} = 0.008$ (in N-body time units) at the influence radius of the black hole. This dimensionless number must afterwards be synchronized with the relevant timescale $t_{\text{cr}}(r_H)$ of the astrophysical galaxy. Consequently $\dot{C}(N) \cdot t_{\text{sim}}$ has to be divided by $t_{\text{cr}}(r_H)$ in order to obtain the number of disrupted stars within the desired physical time unit (e.g yr, Myr) for the black hole of interest:

$$\dot{C}_{\text{astro}} = \frac{0.008 \cdot a(r_{\text{cap}}^{\text{sim}}) N^b}{t_{\text{cr}}(r_H)}. \quad (\text{B5})$$

Our extrapolation formalism strongly depends on the $M_\bullet - \sigma$ relation. More accurate and numerous black hole measurements will improve this relation in the future. Moreover we only treat errors from our simulations and neglected the intrinsic scatter of the $M_\bullet - \sigma$ relation for simplicity.

APPENDIX C: LOSS CONE PROBLEMS

Direct N-body integrations are limited by a maximal computable number of particles which is orders of magnitudes lower compared to particle numbers in the nuclei of astrophysical galaxies. The extrapolation to such astrophysical settings is thus only possible if the relevant physics do not change in between. Loss cone problems (tidal capturing and/or shrinking binary black holes) require special care (Gualandris & Merritt 2007). Here we will show that the inequality

$$T_{\text{refill}} = \theta^2 T_{\text{rel}} \ll H_0^{-1} \quad (\text{C1})$$

is fulfilled up to SMBHs of order $10^7 M_\odot$ and hence our result, $\dot{C} \propto N^{0.83}$, should yield realistic values when extrapolated to such black holes. For black holes much more massive, the situation might change. By assuming the radius r at which particles can enter loss cone orbits without being scattered away through interactions with other stars to

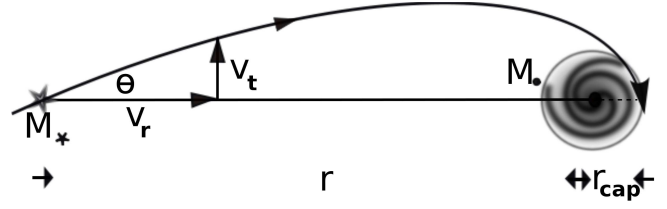


Figure C1. Sketch of a typical loss cone problem.

be $r_{\text{crit}} \approx r_H \Big|_{M_\bullet=10^7 M_\odot}$, the loss cone angle θ can be evaluated from Eq. 1. For the constant of proportionality f we use $f = 2$ in accordance with Frank & Rees (1976). By assuming $r \approx r_H$, $M_\star \approx 1M_\odot$, the relaxation time to be $T_{\text{rel}} \approx H_0^{-1}$ (Freitag et al. 2008) and estimating all other relevant parameters from the $M_\bullet - \sigma$ relation (Ferrarese & Ford 2005), one obtains the desired result $T_{\text{refill}} \approx 4 \cdot 10^{-6} \cdot H_0^{-1} \ll H_0^{-1}$. Even though our assumptions are idealistic and not every star fulfills its plunge into the black hole from the critical radius r_{crit} , it underlines the extrapolation from our numerical simulations to realistic cores of galaxies with central black holes up to $10^7 M_\odot$ to be credible.